

Accelerated Article Preview

FXR inhibition may protect from SARS-CoV-2 infection by reducing ACE2

Received: 3 May 2021

Accepted: 23 November 2022

Accelerated Article Preview

Cite this article as: Brevini, T. et al. FXR inhibition may protect from SARS-CoV-2 infection by reducing ACE2. *Nature* <https://doi.org/10.1038/s41586-022-05594-0> (2022)

Teresa Brevini, Mailis Maes, Gwilym J. Webb, Binu V. John, Claudia D. Fuchs, Gustav Buescher, Lu Wang, Chelsea Griffiths, Marnie L. Brown, William E. Scott III, Pehuén Pereyra-Gerber, William T. H. Gelson, Stephanie Brown, Scott Dillon, Daniele Muraro, Jo Sharp, Megan Neary, Helen Box, Lee Tatham, James Stewart, Paul Curley, Henry Pertinez, Sally Forrest, Petra Mlcochova, Sagar S. Varankar, Mahnaz Darvish-Damavandi, Victoria L. Mulcahy, Rhoda E. Kuc, Thomas L. Williams, James A. Heslop, Davide Rossetti, Olivia C. Tysoe, Vasileios Galanakis, Marta Vila-Gonzalez, Thomas W. M. Crozier, Johannes Bargehr, Sanjay Sinha, Sara S. Upponi, Corrina Fear, Lisa Swift, Kourosh Saeb-Parsy, Susan E. Davies, Axel Wester, Hannes Hagström, Espen Melum, Darran Clements, Peter Humphreys, Jo Herriott, Edyta Kijak, Helen Cox, Chloe Bramwell, Anthony Valentijn, Christopher J. R. Illingworth, UK-PBC research consortium, Bassam Dahman, Dustin R. Bastaich, Raphaella D. Ferreira, Thomas Marjot, Eleanor Barnes, Andrew M. Moon, Alfred S. Barritt IV, Ravindra K. Gupta, Stephen Baker, Anthony P. Davenport, Gareth Corbett, Vassilis G. Gorgoulis, Simon J. A. Buczacki, Joo-Hyeon Lee, Nicholas J. Matheson, Michael Trauner, Andrew J. Fisher, Paul Gibbs, Andrew J. Butler, Christopher J. E. Watson, George F. Mells, Gordon Dougan, Andrew Owen, Ansgar W. Lohse, Ludovic Vallier & Fotios Sampaziotis

This is a PDF file of a peer-reviewed paper that has been accepted for publication. Although unedited, the content has been subjected to preliminary formatting. Nature is providing this early version of the typeset paper as a service to our authors and readers. The text and figures will undergo copyediting and a proof review before the paper is published in its final form. Please note that during the production process errors may be discovered which could affect the content, and all legal disclaimers apply.

1 **FXR inhibition may protect from SARS-CoV-2 infection by reducing ACE2**

2

3 Teresa Brevini*¹, Mailis Maes², Gwilym J. Webb³, Binu V. John⁴, Claudia D. Fuchs⁵, Gustav
4 Buescher⁶, Lu Wang⁷, Chelsea Griffiths⁷, Marnie L. Brown⁷, William E. Scott III⁷, Pehuén
5 Pereyra-Gerber², William T. H. Gelson^{3,8}, Stephanie Brown¹, Scott Dillon¹, Daniele Muraro⁹,
6 Jo Sharp¹⁰, Megan Neary¹⁰, Helen Box¹⁰, Lee Tatham¹⁰, James Stewart¹¹, Paul Curley¹⁰,
7 Henry Pertinez¹⁰, Sally Forrest², Petra Mlcochova^{2,4}, Sagar S. Varankar¹, Mahnaz Darvish-
8 Damavandi^{1,12}, Victoria L. Mulcahy¹³, Rhoda E. Kuc¹⁴, Thomas L. Williams¹⁴, James A.
9 Heslop¹, Davide Rossetti¹, Olivia C. Tysoe^{1,15}, Vasileios Galanakis¹, Marta Vila-Gonzalez¹,
10 Thomas W. M. Crozier², Johannes Bargehr^{1,8,16}, Sanjay Sinha^{1,16}, Sara S. Upponi¹⁷, Corrina
11 Fear¹⁵, Lisa Swift¹⁵, Kourosh Saeb-Parsy^{15,18}, Susan E. Davies¹⁹, Axel Wester²⁰, Hannes
12 Hagström²⁰, Espen Melum²¹⁻²⁵, Darran Clements¹, Peter Humphreys¹, Jo Herriott¹⁰, Edyta
13 Kijak¹⁰, Helen Cox¹⁰, Chloe Bramwell¹⁰, Anthony Valentijn¹⁰, Christopher J. R. Illingworth^{26,27},
14 UK-PBC research consortium²⁸, Bassam Dahman²⁹, Dustin R. Bastaich²⁹, Raffaella D.
15 Ferreira⁴, Thomas Marjot³⁰, Eleanor Barnes³⁰, Andrew M. Moon³¹, Alfred S. Barritt IV³¹,
16 Ravindra K. Gupta^{2,8}, Stephen Baker², Anthony P. Davenport¹⁴, Gareth Corbett³², Vassilis G.
17 Gorgoulis³³⁻³⁵, Simon J. A. Buczacki^{1,12}, Joo-Hyeon Lee^{1,36}, Nicholas J. Matheson^{2,8,31,37},
18 Michael Trauner⁵, Andrew J. Fisher⁷, Paul Gibbs^{15,18}, Andrew J. Butler^{15,18}, Christopher J. E.
19 Watson^{15,18,38}, George F. Mells^{3,13}, Gordon Dougan², Andrew Owen¹⁰, Ansgar W. Lohse⁶,
20 Ludovic Vallier*^{†1,9,39,40} and Fotios Sampaziotis*^{†1,3,8}

21

22 † These authors share senior authorship.

23 *Correspondence to: Fotios Sampaziotis, fs347@cam.ac.uk; Ludovic Vallier,
24 lv255@cam.ac.uk; Teresa Brevini, tb647@cam.ac.uk.

25

1 **Affiliations:**

- 2 1. Wellcome – MRC Cambridge Stem Cell Institute, Cambridge, UK.
- 3 2. Cambridge Institute of Therapeutic Immunology & Infectious Disease (CITIID), Department
4 of Medicine, University of Cambridge, Cambridge, UK.
- 5 3. Cambridge Liver Unit, Cambridge University Hospitals NHS Foundation Trust, Cambridge,
6 UK.
- 7 4. Division of Gastroenterology and Hepatology, University of Miami and Miami VA Health
8 System, Miami, FL
- 9 5. Hans Popper Laboratory of Molecular Hepatology, Division of Gastroenterology and
10 Hepatology, Department of Internal Medicine III, Medical University of Vienna, Austria
- 11 6. Department of Medicine, University Medical Centre Hamburg-Eppendorf, Hamburg,
12 Germany.
- 13 7. Transplant and Regenerative Medicine Laboratory, Translational and Clinical Research
14 Institute, Faculty of Medical Sciences, Newcastle University, Newcastle Upon Tyne, UK.
- 15 8. Department of Medicine, University of Cambridge, Cambridge, UK.
- 16 9. Wellcome Sanger Institute, Wellcome Genome Campus, Hinxton, Cambridge, UK.
- 17 10. Centre of Excellence in Long-acting Therapeutics (CELT), Department of Pharmacology
18 and Therapeutics, Institute of Systems, Molecular and Integrative Biology, University of
19 Liverpool, Liverpool, UK
- 20 11. Department of Infection Biology and Microbiomes, Institute of Infection, Veterinary and
21 Ecological Sciences, University of Liverpool, UK
- 22 12. Nuffield Department of Surgical Sciences, Old Road Campus Research Building, Oxford,
23 UK.
- 24 13. Academic Department of Medical Genetics, University of Cambridge, Cambridge, UK.

- 1 14. Experimental Medicine and Immunotherapeutics, University of Cambridge,
2 Addenbrooke's Hospital, Cambridge, UK.
- 3 15. Department of Surgery, University of Cambridge and NIHR Cambridge Biomedical
4 Research centre, Cambridge, UK.
- 5 16. Division of Cardiovascular Medicine, University of Cambridge, Cambridge, UK.
- 6 17. Department of Radiology, Cambridge University Hospitals NHS Foundation Trust,
7 Cambridge, UK.
- 8 18. Roy Calne Transplant Unit, Cambridge University Hospitals NHS Foundation Trust,
9 Cambridge, UK.
- 10 19. Department of Histopathology, Cambridge University Hospitals NHS Foundation Trust,
11 Cambridge, UK.
- 12 20. Department of Medicine, Huddinge, Karolinska Institutet, Stockholm, Sweden.
- 13 21. Norwegian PSC Research Center, Department of Transplantation Medicine, Division of
14 Surgery, Inflammatory Diseases and Transplantation, Oslo University Hospital,
15 Rikshospitalet, Oslo, Norway.
- 16 22. Research Institute of Internal Medicine, Division of Surgery, Inflammatory Diseases and
17 Transplantation, Oslo University Hospital, Rikshospitalet, Oslo, Norway.
- 18 23. Institute of Clinical Medicine, Faculty of Medicine, University of Oslo, Oslo, Norway.
- 19 24. Section of Gastroenterology, Department of Transplantation Medicine, Division of
20 Surgery, Inflammatory Diseases and Transplantation, Oslo University Hospital,
21 Rikshospitalet, Oslo, Norway.
- 22 25. Hybrid Technology Hub Centre of Excellence, Institute of Basic Medical Sciences, Faculty
23 of Medicine, University of Oslo, Oslo, Norway.
- 24 26. MRC-University of Glasgow Centre for Virus Research, Glasgow, UK.

- 1 27. Department of Applied Mathematics and Theoretical Physics, University of Cambridge,
2 Cambridge, UK.
- 3 28. A list of contributing authors and their affiliations appears at the end of the manuscript.
- 4 29. Department of Health Behavior and Policy, Virginia Commonwealth University,
5 Richmond, VA.
- 6 30. Oxford Liver Unit, Translational Gastroenterology Unit, Oxford University Hospitals NHS
7 Foundation Trust, University of Oxford, Oxford, UK.
- 8 31. Division of Gastroenterology and Hepatology, University of North Carolina, Chapel Hill,
9 NC, USA.
- 10 32. Cambridge University Hospitals NHS Foundation Trust, Cambridge, UK.
- 11 33. Dept. of Histology and Embryology, School of Medicine, National and Kapodistrian
12 University of Athens, Athens, Greece.
- 13 34. Ninewells Hospital and Medical School, University of Dundee, Dundee, UK
- 14 35. Biomedical Research Foundation, Academy of Athens, Athens, Greece.
- 15 36. Department of Physiology, Development and Neuroscience, University of Cambridge,
16 Cambridge, UK.
- 17 37. NHS Blood and Transplant, Cambridge, UK.
- 18 38. National Institute of Health Research (NIHR) Cambridge Biomedical Research
19 Centre, and the NIHR Blood and Transplant Research Unit (BTRU) at the University of
20 Cambridge in collaboration with Newcastle University and in partnership with NHS Blood and
21 Transplant (NHSBT), Cambridge, UK.
- 22 39. Berlin Institute of Health (BIH), BIH Centre for Regenerative Therapies (BCRT), Charité
23 - Universitätsmedizin Berlin, Germany.
- 24 40. Max Planck Institute for Molecular Genetics, Berlin, Germany.

25

1 **Abstract**

2 Prevention of SARS-CoV-2 infection through the modulation of viral host receptors, such as
3 ACE2¹, could represent a new chemoprophylactic approach for COVID-19 complementing
4 vaccination^{2,3}. However, the mechanisms controlling ACE2 expression remain elusive. Here,
5 we identify the farnesoid X receptor (FXR) as a direct regulator of ACE2 transcription in
6 multiple COVID19-affected tissues, including the gastrointestinal and respiratory systems.
7 We then use the over-the-counter compound z-guggulsterone (ZGG) and the off-patent drug
8 ursodeoxycholic acid (UDCA) to reduce FXR signalling and downregulate ACE2 in human
9 lung, cholangiocyte and intestinal organoids and in the corresponding tissues in mice and
10 hamsters. We demonstrate that UDCA-mediated ACE2 downregulation reduces
11 susceptibility to SARS-CoV-2 infection *in vitro*, *in vivo* and in human lungs and livers perfused
12 *ex situ*. Furthermore, we illustrate that UDCA reduces ACE2 expression in the nasal
13 epithelium in humans. Finally, we identify a correlation between UDCA treatment and positive
14 clinical outcomes following SARS-CoV-2 infection using retrospective registry data, and
15 confirm these findings in an independent validation cohort of liver transplant recipients. In
16 conclusion, we identify a novel function of FXR in controlling ACE2 expression and provide
17 evidence that modulation of this pathway could be beneficial for reducing SARS-CoV-2
18 infection, paving the road for future clinical trials.

19

20

21

22

23

24

25

1 **Introduction**

2 Since the beginning of the pandemic, the management of COVID-19 has improved
3 significantly with the development of therapeutic agents, vaccines, and monoclonal
4 antibodies⁴. Despite the transformational impact of vaccines in populations that can access
5 them, significant global health challenges remain. New SARS-CoV-2 variants continue to
6 emerge and are associated with high case rates and substantial global mortality. Treatment
7 options, such as dexamethasone, remdesivir, molnupiravir and nirmatrelvir improve clinical
8 outcome only in specific patient groups^{5,6}; monoclonal antibodies, such as the REGN-COV2
9 cocktail, show reduced neutralising efficacy against new variants⁷, while vaccines are
10 restricted by variable efficacy⁸, the emergence of vaccine-resistant viral variants⁷, cost⁹ and
11 availability¹⁰. Finally, one of the biggest challenges remains prophylaxis in vulnerable and
12 high-risk groups, such as immunocompromised patients who are not expected to mount an
13 appropriate response to vaccines. The only prophylactic agents for these groups are
14 monoclonal antibodies, which are hampered by the propensity of the viral spike to evolve to
15 escape neutralisation⁷. Importantly, there are currently no other approved agents for
16 pharmacological prophylaxis against COVID-19². Therefore, there is a pressing unmet need
17 for novel prophylactic agents that reduce the risk of severe disease³, are less prone to viral
18 resistance and are compatible with healthcare systems in low- and middle-income countries.
19 Viral host receptors represent logical therapeutic targets, because they are essential for
20 SARS-CoV-2 cellular entry and infection¹. Among these, the angiotensin converting
21 enzyme 2 (ACE2), is particularly appealing¹. ACE2 is a transmembrane carboxypeptidase
22 with a broad substrate specificity, including angiotensin II, which acts as the main receptor
23 for SARS-CoV-2. It directly binds the spike protein of different coronaviruses, with a high
24 affinity for SARS-CoV-2, rendering it indispensable for viral entry¹¹. Accordingly, COVID-19

1 predominantly affects tissues expressing ACE2, such as the lungs, the cardiovascular
2 system, the digestive tract and the biliary tree^{12,13}.

3 Modifying ACE2 expression could impede viral entry and protect against infection from
4 SARS-CoV-2 and potentially other coronaviruses using the same receptor. Furthermore,
5 because ACE2 is a host cell protein, its expression is not likely to be affected by mutations
6 in the virus. Therefore, therapies modulating ACE2 expression may be effective against
7 multiple SARS-CoV-2 variants with a higher genetic barrier to resistance. However, the
8 mechanisms controlling ACE2 expression remain elusive. Here, we use human
9 cholangiocyte organoids as a proof-of-principle system to demonstrate that the bile acid
10 receptor farnesoid X receptor (FXR) controls ACE2 expression. We show that this
11 mechanism applies in multiple SARS-CoV-2-affected tissues, including gastrointestinal and
12 respiratory epithelia. Subsequently, we demonstrate that suppressing FXR signalling, with
13 the approved drug ursodeoxycholic acid (UDCA) or the over-the-counter phytosteroid z-
14 guggulsterone (ZGG), reduces ACE2 expression and SARS-CoV-2 infection *in vitro* and in
15 an airborne transmission model in golden Syrian hamsters. We repeat our experiments in
16 human lungs and livers perfused *ex situ* and demonstrate that UDCA administration at
17 physiologically-relevant concentrations reduces ACE2 and viral infection in both organs *ex*
18 *vivo*. We then demonstrate a reduction of ACE2 levels in the nasal epithelium of volunteers
19 receiving clinically approved doses of UDCA. Finally, we interrogate an international registry
20 cohort of patients with COVID-19 and chronic liver disease, identify a correlation between
21 UDCA therapy and better clinical outcomes from COVID-19, and reproduce these results in
22 a second independent cohort of liver transplant recipients.

23

24 **Bile acids modulate cholangiocyte ACE2**

1 To explore the mechanisms controlling ACE2 expression, we used cholangiocyte organoids
2 (COs), as proof-of-principle. Cholangiocytes are epithelial cells lining the lumen of the bile
3 ducts and the gallbladder. We decided to focus on gallbladder cholangiocytes for multiple
4 reasons. Cholangiocytes of the gallbladder express the highest ACE2 levels in the biliary
5 tree¹² (Wilcoxon Rank-Sum test $P < 4.5 \cdot 10^{-201}$) (Extended Data Fig. 1a-d), and one of the highest
6 ACE2 levels in the body¹². Thus, they can be infected by SARS-CoV-2 (Extended Data Fig.
7 1e-f). Furthermore, they can be propagated as organoids¹⁴⁻¹⁶ (Extended Data Fig. 1a-c) and
8 maintain their gallbladder identity *in vitro* (Extended Data Fig. 1a-c) after addition of the bile
9 acid chenodeoxycholic acid (CDCA) in their culture medium¹⁴. The resulting gallbladder
10 cholangiocyte organoids (GCOs) express high levels of ACE2 (Extended Data Fig. 1c; 1g-i),
11 retain their capacity to be infected by SARS-CoV-2 (Extended Data Fig. 2a-e), produce
12 infective viral progeny (Extended Data Fig. 2c), and appropriately upregulate the expression
13 of innate immune genes and antiviral response markers (Extended Data Fig. 2d). Importantly,
14 in the absence of bile acids (CDCA) cholangiocyte organoids lose the expression of
15 gallbladder markers, including ACE2 (Extended Data Fig. 1g-i), which demonstrates that
16 CDCA is required for ACE2 expression. These results not only demonstrate that GCOs
17 provide an appropriate platform to study the mechanisms controlling the expression of ACE2
18 in human cells; they also identify CDCA as a key regulator of SARS-CoV2 receptor levels.

19

20 **Bile acids control ACE2 levels via FXR**

21 Since the bile acid CDCA is the most potent natural agonist of the bile acid receptor and
22 transcription factor FXR¹⁷, we hypothesized that CDCA could control ACE2 expression acting
23 through FXR. To test this hypothesis, we first confirmed that FXR is expressed in gallbladder
24 cholangiocytes *in vivo* and in the corresponding GCOs *in vitro* (Extended Data Fig. 3a-c), and
25 that it is activated by CDCA treatment, as evidenced by the upregulation of its downstream

1 target Small Heterodimer Partner (SHP) (Extended Data Fig. 3c). To confirm that FXR is
2 essential for CDCA-induced ACE2 upregulation, we knocked-down FXR in cholangiocyte
3 organoids using shRNAs, which prevented ACE2 and SHP upregulation following CDCA
4 treatment (Extended Data Fig. 4a-c). To assess whether FXR could bind the ACE2 gene and
5 potentially control its transcriptional activity, we analysed the ACE2 promoter region and
6 identified the presence of the FXR responsive element (FXR RE) IR-1. Accordingly, we
7 confirmed that activated FXR directly binds the ACE2 promoter using chromatin
8 immunoprecipitation (ChIP-QPCR) (Fig. 1a) and showed the functional relevance of this
9 binding using a luciferase reporter containing the ACE2 IR-1 region (Extended Data Fig. 4e-
10 f). Importantly, site-specific mutagenesis on the IR-1 region reduced luciferase signal
11 (Extended Data Fig. 4e-f), demonstrating the specificity of the FXR binding site on the ACE2
12 promoter. Conversely, suppression of FXR signalling, using the FXR antagonist ZGG¹⁸ or the
13 clinically used drug UDCA¹⁷, reduced FXR activity as evidenced by decreased SHP levels
14 (Extended Data Fig. 5a); decreased FXR presence on ACE2 promoter (Fig. 1a; Extended
15 Data Fig. 4e-f); and downregulated the expression of ACE2 at the transcript and protein levels
16 (Fig. 1c-d; Extended Data Fig. 5b-d). Considered together, these results demonstrate that
17 FXR directly controls ACE2 expression in cholangiocytes (Fig. 1b).

18

19 **FXR regulates ACE2 in various cell types**

20 FXR is expressed in multiple cell types^{17,19-21}, and it can be activated by bile acids, which are
21 present not only in the gastrointestinal tract²², but also in the lungs^{20,21} and in the systemic
22 circulation²². Thus, ACE2 regulation through FXR may represent a general mechanism,
23 extending beyond cholangiocytes. To explore this possibility, we repeated our experiments
24 using primary organoids from key organs infected by SARS-CoV-2²³, such as the lungs and
25 the intestine. Importantly, the relevance of these platforms for studying SARS-CoV-2 infection

1 has already been demonstrated^{24,25}. We first confirmed FXR expression in these tissues,
2 both *in vivo* and *in vitro* (Extended Data Fig. 3a-c). Subsequently, we showed that treatment
3 with physiological concentrations of CDCA (10 μ M)²² resulted in FXR activation, evidenced
4 by upregulation of the FXR downstream target SHP (Extended Data Fig. 3c) and increased
5 ACE2 expression (Fig. 1c-d; Extended Data Fig. 5a-c). Conversely, suppression of FXR
6 signalling by UDCA or ZGG reduced ACE2 and SHP levels in primary airway and intestinal
7 organoids (Fig. 1c-d; Extended Data Fig. 5a-d). Importantly, CDCA, UDCA and ZGG
8 exhibited no cytotoxic effects in the concentration range used for our experiments (Extended
9 Data Fig. 5e-f). These results confirm that FXR participates in the regulation of ACE2
10 expression in organoids derived from the respiratory, biliary and intestinal epithelium
11 suggesting that FXR-mediated control of ACE2 expression may be relevant for several
12 organs (Fig. 1b).

14 **FXR regulates viral infection *in vitro***

15 Our results show that suppressing FXR signalling, with the clinically approved drug UDCA,
16 used as first-line treatment in primary biliary cholangitis (PBC)²⁶ or the over-the-counter drug
17 ZGG, reduces ACE2 expression in multiple cell types. To explore the relevance of this finding
18 for COVID-19, we investigated whether FXR-mediated ACE2 downregulation could reduce
19 susceptibility to SARS-CoV-2 infection *in vitro*. For this, we exposed gallbladder
20 cholangiocyte, airway and intestinal organoids to physiological levels of CDCA, to simulate
21 the baseline level of FXR activation present *in vivo*; and infected them with SARS-CoV-2
22 isolated from a patient's nasopharyngeal swab⁴⁵ in the absence or presence of UDCA or
23 ZGG (Fig. 1e-f). Suppression of FXR signalling with UDCA or ZGG reduced viral infection in
24 all three types of organoids (Fig. 1e-f; Extended Data Fig 5a). We then explored whether the
25 observed reduction in viral infection was a direct result of FXR-mediated ACE2

1 downregulation. First, we showed that knock-down of FXR using shRNAs decreases the
2 expression of ACE2 and inhibits viral infection in cholangiocytes organoids independently of
3 the presence of CDCA or UDCA/ZGG (Extended Data Fig. 4d). Accordingly, following
4 knockdown, UDCA or ZGG treatment had no impact on viral infection (Extended Data Fig.
5 4d). Next, to determine whether ACE2 modulation is the only mechanism by which UDCA
6 and ZGG reduce SARS-CoV-2 infection, we treated HEK293T cells genetically engineered
7 to over-express ACE2 independent of FXR²⁷ (Extended Data Fig. 6a-b) with UDCA or ZGG,
8 then infected them with SARS-CoV-2. As expected, in the absence of ACE2 modulation,
9 UDCA and ZGG did not affect viral replication (Extended Data Fig. 6c). Taken together, these
10 results confirm that UDCA and ZGG reduce susceptibility to SARS-CoV-2 infection in multiple
11 cell types *in vitro* via FXR-mediated ACE2 regulation.

13 **FXR regulates viral infection *in vivo***

14 To validate the relevance of these findings *in vivo*, we assessed the effect of UDCA on ACE2
15 expression in FVB/N mice and Syrian Golden Hamsters. We compared ACE2 expression in
16 the respiratory, biliary and intestinal epithelium of 4 mice treated with UDCA vs. 4 control
17 animals not receiving UDCA (Extended Data Fig. 7a). We repeated the same experiment in
18 Syrian Golden Hamsters receiving UDCA (n=3 hamsters) vs. control animals not receiving
19 treatment (n=5 hamsters); and interrogated ACE2 levels in the nasal, respiratory, biliary and
20 intestinal epithelium of these animals (Fig. 2a). Our results demonstrate that UDCA treatment
21 reduces ACE2 expression in mice (Extended Data Fig. 7a-c) and hamsters (Fig. 2a-c;
22 Extended Data Fig. 7d-e).

23 To explore whether UDCA-mediated ACE2 downregulation reduces SARS-CoV-2 infection
24 *in vivo*, we used the well-established Syrian Golden Hamster model of infection. 9 animals
25 were treated with UDCA for 7 days (UDCA group), to achieve plasma concentrations

1 comparable to UDCA levels in patient blood (Extended Data Fig 8a)²⁸. Another 6 animals
2 receiving only the vehicle were used as controls (control group). Neither group was directly
3 infected with the virus (sentinel animals). On day 7 we inoculated n=5 independent, healthy
4 hamsters with the SARS-CoV-2 delta variant (B.1.617.2) via the intranasal route (directly
5 infected animals). Subsequently, each infected animal was co-housed with a group of n=3
6 randomly selected sentinel (uninfected) hamsters from the UDCA or control group for a period
7 of 4 days to interrogate SARS-CoV-2 transmission (Fig. 2a). Viral infection in sentinel animals
8 was assessed with plaque assays from the animal lungs harvested at the end of the
9 experiment (Extended Data Fig. 8b) and confirmed with daily swabs, and viral QPCR in tissue
10 harvested from the lungs and nasal turbinates of the animals at the end of the experiment.
11 Our data demonstrate that UDCA treatment prevented transmission of SARS-CoV-2 in n=6
12 out of 9 sentinel animals (33% infected vs. 67% uninfected); while SARS-CoV-2 was
13 transmitted in n=6 out of 6 (100%) sentinel hamsters receiving vehicle ($P=0.027$; Fisher's
14 exact test) (Fig. 2d-e) for the duration of the experiment. Both directly inoculated and control
15 animals lost weight following viral infection, in contrast to UDCA animals which gained weight
16 (Fig. 2f-g), suggesting a milder course of clinical disease in UDCA treated hamsters. In
17 summary, our *in vivo* results confirm the chemoprophylactic potential of UDCA against
18 COVID19.

19

20 **FXR regulates infection in human organs**

21 We then looked to validate these observations in whole human organs. We focused initially
22 on the lung as one of the primary sites of SARS-CoV-2 infection. To conduct our experiments,
23 we used a pair of human lungs, which was declined for transplantation, and performed *ex*
24 *situ* normothermic perfusion (ESNP) with clinically appropriate mechanical ventilation to
25 oxygenate the lungs *ex vivo* (Fig. 3a). ESNP was developed to objectively assess and

1 potentially improve donor organ function, enhance organ preservation and reduce
2 reperfusion injury by perfusing grafts with warm oxygenated blood (packed red cells) or
3 substitute perfusion solution prior to transplantation^{29,30}. This setting ensured that the lungs
4 remained in near physiological conditions during the experiment³¹. To assess the effect of
5 UDCA, we surgically divided the right and the left lungs from the same donor and we
6 connected them to 2 separate but identical ESNP circuits. This setting allowed us to
7 administer UDCA on one lung (UDCA lung) and use the other lung as a matched control
8 receiving carrier without UDCA (control lung) to facilitate comparison (Fig. 3a).
9 Immediately prior to UDCA administration we measured baseline ACE2 expression in both
10 lungs (0 hours samples collected from lung parenchyma, airway and pulmonary vessels; n=4
11 independent samples from each part of the organ per lung, 24 samples in total; Fig 3b) and
12 ACE2 activity in the circulating perfusate from each ESNP circuit (n=4 independent
13 measurements per circuit; Fig. 3c). We then administered UDCA 'systemically' in the
14 perfusate of the UDCA lung; UDCA was diluted in saline to 2000 ng/ml corresponding to the
15 steady-state plasma concentration achieved in patients after multiple doses of oral UDCA²⁸.
16 At the same time the control lung received an equal volume of saline (carrier) (Fig 3a; 0 hours
17 = UDCA/Carrier administration). We continued *ex situ* perfusion with UDCA for 6 hours.
18 Repeat perfusate and tissue samples were collected at 6 hours, matching our pre-UDCA
19 measurements (n=24 independent tissue samples and n=8 independent perfusate samples
20 per timepoint). We observed that *ex vivo* treatment with UDCA reduced ACE2 expression in
21 lung parenchyma, airway and pulmonary vessels and ACE2 activity in the perfusate,
22 compared to the carrier control (Fig. 3b-c).
23 We then assessed the importance of this reduction in ACE2 on susceptibility to SARS-CoV-
24 2 infection. We infected samples from the lung parenchyma, airway and vessels of each lung
25 6 hours after UDCA or carrier administration (n=4 parenchymal, n=4 bronchial, n=4

1 pulmonary vessel independent samples per lung; see methods) and observed that UDCA
2 treatment reduced SARS-CoV-2 infection (Fig. 3d-e). These results validate that clinical
3 doses of circulating UDCA can downregulate ACE2 levels and reduce SARS-CoV-2 infection
4 in human lungs *ex vivo*.

5 Importantly, FXR inhibitors are metabolized by the liver, and ultimately distributed to different
6 tissues through the systemic circulation. To simulate this process, we repeated ESNP with 2
7 human liver grafts (Extended Data Fig. 9a; see methods). One liver was perfused with UDCA
8 (2000 ng/ml), while the other was perfused with carrier and served as a control. In keeping
9 with our lung findings, we observed that 'systemic' UDCA treatment lowered ACE2 in the
10 circulating perfusate (Extended Data Fig. 9b) and in gallbladder cholangiocytes (n=4
11 independent samples from the grafts' gallbladder per timepoint) (Extended Data Fig. 9c-d)
12 and reduced SARS-CoV-2 infection in gallbladder cholangiocytes (Extended Data Fig. 9e-f).
13 These results confirm that suppression of FXR signalling via systemic administration of the
14 approved drug UDCA can downregulate ACE2 in the circulating perfusate and tissue (lung
15 parenchyma, bronchi, vessels, gallbladder epithelium) of machine-perfused organs and
16 reduce SARS-CoV-2 infection *ex vivo*.

17

18 **UDCA reduces ACE2 in humans**

19 Our previous results encouraged us to assess the potential impact of UDCA on ACE2 levels
20 in humans. Given the favourable safety profile, lack of side effects and limited cost of UDCA,
21 we recruited 8 volunteers from the University Medical Centre Hamburg-Eppendorf and
22 treated them with UDCA at the standard therapeutic dosage of 15 mg/kg/day²⁶ for 5 days
23 (Supplementary Table S5). The volunteers' nasal epithelial cells were collected using
24 nasopharyngeal swabs and ACE2 levels were measured at multiple timepoints before, during
25 and after treatment with UDCA (see methods, Fig. 4a). Participants with non-detectable

1 cellular RNA in their nasopharyngeal swabs were excluded (n=2). Our results showed that in
2 humans, UDCA reduces ACE2 levels in the nasal epithelium, which is a prime site of SARS-
3 CoV-2 infection (Fig. 4b).

4 To validate our findings further, we took advantage of the drug's extensive use for cholestatic
5 liver disorders (e.g., first-line treatment for the cholestatic autoimmune disorder primary
6 biliary cholangitis, PBC). We interrogated a published serum proteomics dataset from the
7 UK-PBC patient cohort³², comparing ACE2 levels in the serum of UDCA naïve patients
8 (n=62) vs. patients receiving UDCA (n=308). We observed that UDCA correlates with lower
9 serum ACE2 levels after linear regression for age, sex, body mass index (BMI), stage of liver
10 disease (Child-Turcotte-Pugh class) and alkaline phosphatase (ALP) ($P = 0.007$; Extended
11 Data Fig. 10a-b; see methods), validating our previous findings (Supplementary Table S5;
12 Supplementary File S1)..

14 **UDCA may improve COVID-19 outcome**

15 Based on these observations, we decided to explore the potential impact of UDCA treatment
16 on the outcome of COVID-19 in patients. For this, we interrogated the COVID-Hep/SECURE-
17 Liver registries^{33,34}. These registries comprise data of patients with chronic liver disease
18 (n=1,096) who developed COVID-19, including patients with cholestatic liver disorders
19 receiving UDCA (n=31) (Fig. 4c) (Supplementary Table S7 and S8). We observed that,
20 accepting the potential for selection bias in case reporting, patients receiving UDCA had
21 better outcomes compared to patients not receiving UDCA, including reduced hospitalisation,
22 ICU admission and death (Fig. 4d), after propensity score matching (No UDCA:UDCA=5:1)
23 for sex, age, diabetes, stage of liver disease (Child-Turcotte-Pugh class),
24 immunosuppression, chronic pulmonary disease and non-alcoholic fatty liver disease
25 (NAFLD) (Fig. 4d). We note that propensity score matching was not possible for alcohol-

1 related liver disease (ARLD), therefore these patients were excluded from the analysis (see
2 methods). We then sought to replicate these results in a second independent patient cohort.
3 For this, we interrogated liver transplant recipients in the Veterans Outcomes and Costs
4 Associated with Liver disease (VOCAL) cohort who received at least two doses of a COVID-
5 19 mRNA vaccine. Of 119 vaccinated participants that developed COVID-19, n=24 were
6 receiving UDCA (Supplementary Table S9). These 24 participants on UDCA were matched
7 with 72 who were not on UDCA (No UDCA:UDCA=3:1) for sex, age, ethnicity, BMI, location
8 within the United States, diabetes, chronic pulmonary disease, the type of
9 immunosuppression (calcineurin inhibitor therapy, with or without anti-metabolite therapy)
10 and the dominant SARS-CoV-2 variant at time of infection (Fig. 4e). We observed that,
11 accepting the potential for selection bias in case reporting, patients on UDCA were less likely
12 to develop moderate, severe or critical COVID-19 ($P=0.026$) (Fig. 4f) according to the
13 National Institute of Health COVID-19 severity score³⁵. Importantly, during the publication of
14 this manuscript, we became aware of an independent study interrogating the association of
15 exposure of UDCA and outcomes of COVID-19, among participants in the VOCAL cohort
16 with cirrhosis. In this analysis, 1607 participants with cirrhosis and UDCA exposure were
17 propensity score matched with 1607 participants with cirrhosis but without UDCA exposure.
18 The authors found that on multivariable logistic regression, UDCA exposure was associated
19 with a 46% reduced odds of developing COVID-19 (adjusted Odds ratio [aOR] 0.54, 95% CI
20 0.41- 0.71, $p<0.0001$). The association was observed across the spectrum of COVID-19
21 against symptomatic illness (aOR 0.54, 95% CI 0.39-0.73, $p<0.0001$), at least moderate
22 COVID-19 (aOR 0.51, 95% CI 0.32-0.81, $p=0.005$), and severe or critical COVID-19 (aOR
23 0.48, 95% CI 0.25-0.94, $p=0.03$). These results provide additional independent evidence
24 reinforcing our study. Taken together, the findings from our exploratory and validation cohorts

1 support further investigation of the impact of UDCA on clinical outcomes of COVID-19 in a
2 large prospective clinical trial.

3

4 **Discussion**

5 Considered collectively, our findings demonstrate that FXR participates in the regulation of
6 ACE2 expression in multiple tissues involved in SARS-CoV-2 replication. Suppression of
7 FXR activity, using the clinically approved drug UDCA, downregulates ACE2 expression and
8 reduces SARS-CoV-2 infection *in vitro*, *in vivo* and *ex vivo*. Furthermore, our clinical
9 observations indicate that UDCA reduces ACE2 levels in the nasal epithelium of healthy
10 individuals and suggest a potential correlation between UDCA and positive clinical outcomes
11 in COVID-19 patients.

12 The finding that FXR regulates ACE2 is novel but not entirely surprising. The functions of
13 ACE2 as a molecular chaperone for the amino acids transporter SLC6A19 and as a peptidase
14 justify its presence in the GI tract and suggest a potential role in digestion. Accordingly, the
15 upregulation in ACE2 expression by FXR, which is activated by bile, a digestive fluid, may
16 reflect a mechanism to increase peptidase levels and amino acids absorption during
17 digestion. Furthermore, in addition to its role in the GI system, FXR is expressed in multiple
18 organs, including the lungs^{20,21}, with a broad variety of functions, ranging from bile acid²² and
19 lipid metabolism³⁶, to glucose homeostasis³⁷, fibrosis³⁸ and inflammation³⁹. Importantly, its
20 natural ligands, such as bile acids and hormones⁴⁰ (e.g., androgens) are present in the
21 systemic circulation²²; and it is the therapeutic target of several approved drugs¹⁷. This broad
22 expression and function explain how FXR could regulate ACE2 in multiple tissues beyond
23 the biliary tree.

24 Our results illustrate the potential of ACE2 modulation as a novel host-directed treatment
25 which might be efficacious as primary and secondary prophylaxis in COVID-19. These

1 findings are in keeping with existing studies illustrating the benefits of targeting the virus-host
2 interaction for SARS-CoV-2 at the level of ACE2¹ or the spike protein⁷. Indeed, large
3 Mendelian randomization analyses in over 7,554 patients hospitalised with COVID-19 and
4 more than 1 million controls demonstrated that higher ACE2 levels strongly correlated with
5 increased risk of COVID-19 hospitalisation, identifying ACE2 as a logical candidate for drug
6 development in COVID19¹. Additionally, the extensive clinical literature supporting
7 Ronapreve and Evusheld, both dual combinations of monoclonal antibodies against the
8 SARS-CoV-2 spike protein, demonstrates the utility of inhibiting the viral spike protein-ACE2
9 interaction for prophylaxis and treatment in COVID19 for susceptible pre-Omicron
10 variants^{41,42}. However, targeting the viral spike protein with monoclonal antibodies is limited
11 by diversity and evolution of the viral spike sequences, rendering many of these agents
12 ineffective against new SARS-CoV-2 variants⁷. Conversely, targeting ACE2 is advantageous
13 for multiple reasons. ACE2 modulation is a host-directed treatment, which does not target
14 the virus. Such mechanisms may present a higher barrier to emergence of resistance
15 although this has yet to be empirically demonstrated. Furthermore, since ACE2 is a critical
16 mechanism for cell entry, the approach maybe more resilient as variants continue to
17 emerge⁴³. Finally, ACE2 is a common receptor for multiple coronaviruses, such as SARS-
18 CoV and HCoV-NL63. Confirmation of the efficacy of this strategy may therefore provide a
19 quickly deployable intervention in the event of future coronavirus outbreaks. Taken
20 collectively with our own observations on the effects of ACE2 modulation for SARS-CoV-2
21 infection, these points illustrate that ACE2 modulators warrant consideration as priority
22 candidates for clinical evaluation in COVID-19 trials¹.

23 Our finding that FXR signalling suppression through UDCA or ZGG reduces ACE2
24 expression, and limits SARS-CoV-2 infection, identifies a new potential clinical application for
25 FXR inhibitors, but also raises some points for consideration. First, FXR activation decreases

1 inflammation by modulating NFkB in multiple organs⁴⁴, including lungs²¹, liver¹⁷ and
2 intestine¹⁷. Conversely, UDCA has been shown to reduce inflammation in multiple tissues,
3 including lung, in an FXR-independent fashion⁴⁵. Given the complex interplay between FXR,
4 UDCA and inflammation⁴⁶, the balance of benefits for FXR activation in terms of SARS-CoV-
5 2 infection and inflammation should be carefully considered. It is possible that FXR
6 suppressors, beyond UDCA, which lack anti-inflammatory effects would be better suited for
7 prophylaxis or early intervention and not indicated for severe disease with ongoing tissue
8 inflammation⁴⁷. Second, our study suggests that FXR activators used in clinical practice, such
9 as obeticholic acid (OCA) may increase the risk of developing COVID-19 by upregulating
10 ACE2 in healthy individuals. Conversely, in liver patients OCA may paradoxically prevent
11 COVID-19 by reducing disease severity and ameliorating cholestasis, resulting in a net
12 reduction of FXR activity. Therefore, further studies are needed to elucidate these points.
13 Our results identify UDCA as a particularly advantageous modulator of ACE2 levels, for use
14 in COVID-19. We demonstrated that UDCA reduces SARS-CoV-2 infection *in vitro*, *in vivo*
15 and *ex vivo*; and lowers ACE2 expression in the nasal epithelium of healthy volunteers.
16 Although our animal data do not exclude that UDCA delays SARS-CoV-2 transmission
17 beyond the duration of our experiments; our patient data illustrate that this does not change
18 the net effect of reducing disease severity, which make it particularly attractive for
19 investigation as pharmacological prophylaxis against SARS-CoV-2 infection. Compared to
20 other agents, such as vaccines and monoclonals, it is easy to administer orally, easily stored,
21 affordable and accessible to health systems world-wide for large scale production, as it is off
22 patent. In addition, UDCA is well-tolerated, has limited drug- drug interactions, and a
23 favourable safety profile enabling it to be administered for long periods of time. Of note,
24 UDCA is already administered long-term for different clinical indications to vulnerable groups
25 that would benefit from chemoprophylaxis, such as bone marrow and liver transplant patients,

1 for prevention of veno-occlusive disease⁴⁸ and treatment of cholangiopathy²⁶ respectively. It
2 has excellent tolerability and minimal side effects in these patient groups^{26,48} demonstrating
3 the potential feasibility of using UDCA as pharmacological prophylaxis against COVID19 in
4 vulnerable groups. Nevertheless, our study is not a clinical trial and therefore we cannot
5 exclude the potential for confounding and selection biases. Consequently, it will be imperative
6 to validate these results in prospective double blinded clinical trials and fully assess the
7 impact of this drug on ACE2 levels and susceptibility to SARS-CoV-2 infection. For the
8 absence of doubt, the authors do not support use of UDCA for COVID19 until appropriate
9 policy informed by robust clinical evidence is available. The authors also do not condone the
10 use of UDCA as a substitute for highly effective vaccinations in patients for which they are
11 indicated.

12 Finally, we demonstrated that UDCA could reduce ACE2 levels and SARS-CoV-2 infection
13 in machine perfused organs. This is one of the first studies testing the effect of a drug in a
14 whole human organ perfused *ex situ*. This finding could prove important for organ
15 transplantation, especially given concerns about peri-operative viral transmission⁴⁹.
16 Furthermore, although more data are required to definitively establish this approach, our work
17 sets the stage for future studies using machine-perfused organs for pharmacological studies.
18 In conclusion, these results validate CDCA-treated cholangiocytes organoids as a novel
19 platform for disease modelling and drug testing against SARS-CoV-2 infection; identify FXR
20 as a new therapeutic target in the management of COVID-19 and open up new avenues for
21 the modulation of ACE2 through FXR for prevention of SARS-CoV-2 infection as well as other
22 viruses using ACE2 for cell entry.

23

24 **References**

25 1. Gaziano, L. *et al.* Actionable druggable genome-wide Mendelian randomization

- 1 identifies repurposing opportunities for COVID-19. *Nat. Med.* **27**, 668–676 (2021).
- 2 2. World Health Organization. WHO Guidelines: Drugs to prevent COVID-19. *WHO*
3 *Guidel.* **53**, 1689–1699 (2021).
- 4 3. Bartoszko, J. J. *et al.* Prophylaxis against covid-19: Living systematic review and
5 network meta-analysis. *BMJ* **373**, 1–12 (2021).
- 6 4. Organization., W. H. Therapeutics and COVID-19 LIVING GUIDELINE 3 MARCH
7 2022. 1–109 (2022).
- 8 5. The RECOVERY Collaborative Group. Dexamethasone in Hospitalized Patients with
9 Covid-19. *N. Engl. J. Med.* **384**, 693–704 (2021).
- 10 6. Beigel, J. H. *et al.* Remdesivir for the Treatment of Covid-19 — Final Report. *N. Engl.*
11 *J. Med.* **383**, 1813–1826 (2020).
- 12 7. Cao, Y. *et al.* Omicron escapes the majority of existing SARS-CoV-2 neutralizing
13 antibodies. *Nature* **602**, 657–663 (2022).
- 14 8. Collier, D. A. *et al.* Sensitivity of SARS-CoV-2 B.1.1.7 to mRNA vaccine-elicited
15 antibodies. *Nature* (2021) doi:10.1038/s41586-021-03412-7.
- 16 9. Dyer, O. Covid-19: Countries are learning what others paid for vaccines. *Bmj* n281
17 (2021) doi:10.1136/bmj.n281.
- 18 10. Callaway, E. The unequal scramble for coronavirus vaccines — by the numbers.
19 *Nature* **584**, 506–507 (2020).
- 20 11. Zhou, P. *et al.* A pneumonia outbreak associated with a new coronavirus of probable
21 bat origin. *Nature* **579**, 270–273 (2020).
- 22 12. Sungnak, W. *et al.* SARS-CoV-2 entry factors are highly expressed in nasal epithelial
23 cells together with innate immune genes. *Nat. Med.* **26**, 681–687 (2020).
- 24 13. Evangelou, K. *et al.* Pulmonary infection by SARS-CoV-2 induces senescence
25 accompanied by an inflammatory phenotype in severe COVID-19: possible

- 1 implications for viral mutagenesis. *Eur. Respir. J.* **60**, (2022).
- 2 14. Sampaziotis, F. *et al.* Cholangiocyte organoids can repair bile ducts after
3 transplantation in the human liver. *Science* **371**, 839–846 (2021).
- 4 15. Tysoe, O. C. *et al.* Isolation and propagation of primary human cholangiocyte
5 organoids for the generation of bioengineered biliary tissue. *Nature Protocols* vol. 14
6 (Springer US, 2019).
- 7 16. Sampaziotis, F. *et al.* Reconstruction of the mouse extrahepatic biliary tree using
8 primary human extrahepatic cholangiocyte organoids. *Nat. Med.* **23**, 954–963 (2017).
- 9 17. Sun, L., Cai, J. & Gonzalez, F. J. The role of farnesoid X receptor in metabolic
10 diseases, and gastrointestinal and liver cancer. *Nat. Rev. Gastroenterol. Hepatol.*
11 **0123456789**, (2021).
- 12 18. Urizar, N. L. *et al.* A natural product that lowers cholesterol as an antagonist ligand for
13 FXR. *Science (80-.).* **296**, 1703–1706 (2002).
- 14 19. Sun, L. *et al.* Gut microbiota and intestinal FXR mediate the clinical benefits of
15 metformin. *Nat. Med.* **24**, 1919–1929 (2018).
- 16 20. Chen, B. & Hou-Rong Cai, Shan Xue, Wen-Jie You, Bin Liu, H.-D. J. Bile acids
17 induce activation of alveolar epithelial cells and lung fibroblasts through farnesoid X
18 receptor-dependent and independent pathways. *Respirology* **21**, 1075–80 (2016).
- 19 21. Comeglio, P. *et al.* Anti-fibrotic effects of chronic treatment with the selective FXR
20 agonist obeticholic acid in the bleomycin-induced rat model of pulmonary fibrosis. *J.*
21 *Steroid Biochem. Mol. Biol.* **168**, 26–37 (2017).
- 22 22. Fickert, P. & Wagner, M. Biliary bile acids in hepatobiliary injury – What is the link? *J.*
23 *Hepatol.* **67**, 619–631 (2017).
- 24 23. Gupta, A. *et al.* Extrapulmonary manifestations of COVID-19. *Nat. Med.* **26**, 1017–
25 1032 (2020).

- 1 24. Youk, J. *et al.* Three-Dimensional Human Alveolar Stem Cell Culture Models Reveal
2 Infection Response to SARS-CoV-2. *Cell Stem Cell* **27**, 905-919.e10 (2020).
- 3 25. Lamers, M. M. *et al.* SARS-CoV-2 productively infects human gut enterocytes.
4 *Science (80-.)*. **3**, 50–54 (2020).
- 5 26. EASL Clinical Practice Guidelines. EASL Clinical Practice Guidelines: The diagnosis
6 and management of patients with primary biliary cholangitis. *J. Hepatol.* **67**, 145–172
7 (2017).
- 8 27. Gerber, P. P. *et al.* A protease-activatable luminescent biosensor and reporter cell
9 line for authentic SARS-CoV-2 infection. *PLoS Pathog.* **18**, 1–23 (2022).
- 10 28. Lee, S. *et al.* Pharmacokinetics of Ursodeoxycholic Acid in Elderly Volunteers
11 Compared With Younger Adults in a Korean Population. *J. Clin. Pharmacol.* **59**,
12 1085–1092 (2019).
- 13 29. Nasralla, D. *et al.* A randomized trial of normothermic preservation in liver
14 transplantation. *Nature* **557**, 50–56 (2018).
- 15 30. Andreasson, A. S. I., Dark, J. H. & Fisher, A. J. Ex vivo lung perfusion in clinical lung
16 transplantation-State of the art. *Eur. J. Cardio-thoracic Surg.* **46**, 779–788 (2014).
- 17 31. Watson, C. J. E. *et al.* Observations on the ex situ perfusion of livers for
18 transplantation. *Am. J. Transplant.* **18**, 2005–2020 (2018).
- 19 32. Barron-Millar, B. *et al.* The Serum Proteome and Ursodeoxycholic Acid Response in
20 Primary Biliary Cholangitis. *Hepatology* **0**, 1–15 (2021).
- 21 33. Webb, G. J. *et al.* Outcomes following SARS-CoV-2 infection in liver transplant
22 recipients: an international registry study. *Lancet Gastroenterol. Hepatol.* (2020)
23 doi:10.1016/S2468-1253(20)30271-5.
- 24 34. Marjot, T. *et al.* Outcomes following SARS-CoV-2 infection in patients with chronic
25 liver disease: An international registry study. *J. Hepatol.* **74**, 567–577 (2021).

- 1 35. John, B. V. *et al.* Effectiveness of COVID-19 Viral Vector Ad.26.COV2.S Vaccine and
2 Comparison with mRNA Vaccines in Cirrhosis. *Clin. Gastroenterol. Hepatol.* 1–7
3 (2022) doi:10.1016/j.cgh.2022.05.038.
- 4 36. Patel, K. *et al.* Cilofexor, a Nonsteroidal FXR Agonist, in Patients With Noncirrhotic
5 NASH: A Phase 2 Randomized Controlled Trial. *Hepatology* **72**, 58–71 (2020).
- 6 37. Jiang, C. *et al.* Intestinal farnesoid X receptor signaling promotes nonalcoholic fatty
7 liver disease. *J. Clin. Invest.* **125**, 386–402 (2015).
- 8 38. Zhao, K. *et al.* Activation of FXR protects against renal fibrosis via suppressing
9 Smad3 expression. *Sci. Rep.* **6**, 1–8 (2016).
- 10 39. Gadaleta, R. M. *et al.* Farnesoid X receptor activation inhibits inflammation and
11 preserves the intestinal barrier in inflammatory bowel disease. *Gut* **60**, 463–472
12 (2011).
- 13 40. Caron, S., Cariou, B. & Staels, B. FXR: More than a bile acid receptor?
14 *Endocrinology* **147**, 4022–4024 (2006).
- 15 41. Weinreich, D. M. *et al.* REGN-COV2, a Neutralizing Antibody Cocktail, in Outpatients
16 with Covid-19. *N. Engl. J. Med.* **384**, 238–251 (2021).
- 17 42. Levin, M. J. *et al.* Intramuscular AZD7442 (Tixagevimab-Cilgavimab) for Prevention of
18 Covid-19. *N. Engl. J. Med.* 1–13 (2022) doi:10.1056/NEJMoa2116620.
- 19 43. Kemp, S. A. *et al.* SARS-CoV-2 evolution during treatment of chronic infection.
20 *Nature* **592**, (2021).
- 21 44. Fiorucci, S., Biagioli, M., Zampella, A. & Eleonora Distrutti. Bile Acids Activated
22 Receptors Regulate Innate Immunity. *Front. Immunol.* **13**, (2018).
- 23 45. Sharma, R. *et al.* Ursodeoxycholic acid amides as novel glucocorticoid receptor
24 modulators. *J. Med. Chem.* **54**, 122–130 (2011).
- 25 46. Fuchs, C. D. & Trauner, M. Role of bile acids and their receptors in gastrointestinal

- 1 and hepatic pathophysiology. *Nat. Rev. Gastroenterol. Hepatol.* **0123456789**, (2022).
- 2 47. Vabret, N. *et al.* Immunology of COVID-19: Current State of the Science. *Immunity*
3 **52**, 910–941 (2020).
- 4 48. Mohty, M. *et al.* Prophylactic, preemptive, and curative treatment for sinusoidal
5 obstruction syndrome/veno-occlusive disease in adult patients: a position statement
6 from an international expert group. *Bone Marrow Transplant.* **55**, 485–495 (2020).
- 7 49. Qin, J. *et al.* Perioperative Presentation of COVID-19 Disease in a Liver Transplant
8 Recipient. *Hepatology* **72**, 1491–1493 (2020).
- 9

10 **Figure Legends**

11 **Figure 1. FXR modulates ACE2 expression and SARS-CoV-2 infection.** (a) Chromatin
12 immunoprecipitation followed by QPCR (ChIP-QPCR) on cholangiocyte organoids showing
13 that the FXR agonist (CDCA) promotes binding of FXR on the ACE2 promoter which is
14 reduced by FXR inhibitors (UDCA/ZGG). OST α as positive control; ACE2 promoter adjoining
15 region as negative control; n=4 independent experiments; one-way ANOVA adjusted for
16 multiple comparisons; bars, standard deviation. (b) Schematic representation of the
17 suggested mechanism for FXR-mediated control of ACE2 expression and SARS-CoV-2
18 infection relative to panels (e-f). (c-d) QPCR (c) and immunofluorescence (d) showing ACE2
19 levels upon modulation of FXR activity in primary airway, biliary and intestinal organoids.
20 Housekeeping gene, PBGD; n=4 independent experiments; one-way ANOVA; centre line,
21 median; box, interquartile range (IQR); whiskers, range; bars, standard deviation. Yellow
22 scale bars 50 μ m; grey scale bars 25 μ m. (e) QPCR quantifying SARS-CoV-2 viral RNA 24
23 hours post infection (hpi) in primary organoids treated with physiological levels of bile acids
24 (CDCA) in the presence or absence of FXR inhibitors (UDCA/ZGG). Housekeeping gene,
25 GAPDH; n=4 independent experiments; one-way ANOVA adjusted for multiple comparisons;

1 centre line, median; box, interquartile range (IQR); whiskers, range; bars, standard deviation.
2 (f) Immunofluorescence images demonstrating presence of SARS-CoV-2 spike protein 24
3 hpi in organoids corresponding to (e). Scale bars 25 μm . (CDCA, UDCA and ZGG
4 concentration, 10 μM).

5
6 **Figure 2 FXR inhibition reduces ACE2 and SARS-CoV-2 infection *in vivo*.** (a) Schematic
7 of the experiment performed in Syrian golden hamsters. Sentinel animals were not directly
8 inoculated with virus. SARS-CoV-2 infection in sentinels was achieved through transmission
9 from directly inoculated animals after co-housing. (b) QPCR showing that treatment with
10 UDCA reduces ACE2 levels in hamster nasal turbinates and lungs. Housekeeping gene,
11 GAPDH; n=5 vehicle/No UDCA group vs n=3 UDCA group; unpaired two-tailed t-test; centre
12 line, median; box, interquartile range; whiskers, range; bars, standard deviation. (c)
13 Immunofluorescence images showing ACE2 levels in nasal and respiratory epithelium of
14 hamsters receiving UDCA vs. vehicle. N=3 hamsters/group. Scale bars 100 μm . (d) QPCR
15 showing SARS-CoV-2 RNA levels in swabs, nasal turbinates and lungs of directly inoculated
16 hamsters and sentinel animals treated with UDCA/vehicle and co-housed with infected
17 animals. Samples were collected after 4 days of co-housing. SARS-CoV-2 nucleocapsid RNA
18 quantification relative to 18s. N=3 hamsters/group; n=9 UDCA animals vs n=6 vehicle
19 animals; animals from each experiment are represented with different symbols; Kruskal-
20 Wallis test adjusted for multiple comparisons. (e) Kaplan-Meier curve showing the
21 percentage of animals with a PCR positive swab for SARS-CoV-2 over the course of the
22 experiment outlined in panel (a). N=9 UDCA, n=6 vehicle, n=5 directly inoculated animals;
23 Log-rank Mantel cox test comparing UDCA vs vehicle. (f) Percentage weight change from
24 the start of the experiment outlined in panel (a). Bars, range. Day 0 corresponds to the start
25 of co-housing. (g) Percentage weight change after SARS-CoV-2 infection in sentinel animals.

1 The time of infection was defined as the earliest day a sentinel animal developed a positive
2 swab (day 3 for both UDCA/vehicle groups). N=3 independent experiments; n=9 UDCA, n=6
3 vehicle, n=5 directly inoculated animals; unpaired two-tailed t-test; centre line, median; box,
4 interquartile range; whiskers, range; bars, standard deviation.

5
6 **Figure 3. FXR inhibition reduces ACE2 levels and SARS-CoV-2 infection in a human**
7 **lung ex vivo.** (a) Schematic representation of the lung *ex situ* normothermic perfusion
8 (ESNP) experiment performed; including type of samples harvested and timeline. 0h: 0 hours
9 baseline sample collection and UDCA/carrier administration. The 0h samples were collected
10 prior to UDCA administration. 6h: 6 hours after UDCA/carrier administration. For each
11 timepoint, 4 independent tissue samples were obtained from the lung parenchyma (alveoli),
12 the airways and the vessels for each lung and used for ACE2 measurement and viral infection
13 (n=4 lung parenchyma, n=4 airway and n=4 pulmonary vessel samples per lung per
14 timepoint). (b) QPCR demonstrating that UDCA treatment reduces ACE2 levels in human
15 alveoli, airway and pulmonary vessels perfused *ex situ*. Housekeeping gene, GAPDH; n=4
16 independent samples; unpaired two-tailed t-test; centre line, median; box, interquartile range
17 (IQR); whiskers, range; error bars, standard deviation. (c) ACE2 enzymatic activity in the
18 perfusate demonstrating that UDCA reduces ACE2. N=4 independent samples; unpaired
19 two-tailed t-test; centre line, median; box, interquartile range (IQR); whiskers, range; bars,
20 standard deviation. (d) QPCR showing that 6h of ESNP with UDCA reduces SARS-CoV-2
21 infection in human alveoli, airway and pulmonary vessels *ex vivo*. Housekeeping gene,
22 GAPDH. N=4 independent samples; unpaired two-tailed t-test. (e) Immunofluorescence
23 staining for ACE2 and SARS-CoV-2 in human alveoli, airway and pulmonary vessels
24 following ESNP with UDCA/carrier. N=4 independent samples. White scale bars 100 μm ,
25 yellow scale bars 50 μm . (UDCA, concentration, 2000 ng/ml). L, lumen.

1
2
3
4
5
6
7
8
9
10
11
12
13
14
15
16
17
18
19
20
21
22
23
24

Figure 4. UDCA is associated with lower ACE2 levels and better clinical outcome in COVID-19 patients. (a-b) Schematic representation of the study design. 6 healthy individuals received 15 mg/kg/day of UDCA for 5 days. ACE2 levels were measured via QPCR in nasal epithelial cells collected via nasopharyngeal swabs. Day 0 corresponds to samples collected immediately before starting UDCA treatment. Samples were collected daily during drug administration and again at day 22-23 and 24-28 to assess the washout of UDCA. (b) QPCR measurement of ACE2 levels in nasal epithelial cells collected with nasopharyngeal swabs. Each dot represents one individual measurement, lines connect dots from the same individual (n=6). Housekeeping gene, GAPDH; n=6 individuals; one-way ANOVA with Geisser-Greenhouse's correction. Please, refer to Supplementary Table S5 for participant characteristics. (c) Schematic overview of the analysis performed in the exploratory cohort corresponding to panel (d). (d) Propensity-score matched analyses showing major outcomes following SARS-CoV-2 infection in patients taking UDCA compared to non-UDCA controls. N=155 patients not on UDCA; n=31 patients on UDCA. Please, refer to Supplementary Table S6 and S7 for patient characteristics. Bars, 95% confidence interval. (e) Schematic overview of the analysis performed in the validation cohort corresponding to panel (f). (f) Propensity-score matched analyses showing disease severity following SARS-CoV-2 infection in patients taking UDCA compared to non-UDCA controls using the NIH COVID-19 severity score. Moderate +, moderate, severe or critical disease; severe +, severe or critical disease. N=72 patients not on UDCA; n=24 patients on UDCA. Please, refer to Supplementary Table S8 for patient characteristics. Bars, 95% confidence interval.

1 **Methods**

2 **Ethical approval**

3 All human samples were obtained from patients, deceased transplant organ donors or liver
4 explants with informed consent for use in research, and ethical approval (Research Ethics
5 Committee - REC 09/H0305/68; 14/NW/1146; 15/EE/0152; 15/WA/0131; 18/EE/0269; and
6 Papworth Hospital Research Tissue Bank project number T02233). The mouse animal study
7 was approved by the Animal Ethics Committee of the Medical University of Vienna and the
8 Federal Ministry of Science, Research and Economy (BMWFW-66.009/0008-WF/3b/2015)
9 and was performed according to the Animal Research: Reporting of In Vivo Experiments
10 (ARRIVE) guidelines. The hamster animal study was approved by the University of Liverpool
11 Animal Welfare and Ethical Review Board and performed under UK Home Office licences
12 (PP9284915 and PP4715265) and it was completed at the University of Liverpool and
13 conducted in accordance with the UK Home Office Animals Scientific Procedures Act (ASPA,
14 1986). Human lungs and livers retrieved for transplantation but subsequently declined were
15 used for *ex situ* normothermic perfusion experiments (National Research Ethics Committee
16 (NREC) North East – Newcastle and North Tyneside 16/NE/0230, lung; NREC East of
17 England – Cambridge East 14/EE/0137, liver). The study involving volunteers from the
18 University Medical Centre Hamburg-Eppendorf was performed with informed consent and
19 ethical approval (Ethik-Kommission der Ärztekammer Hamburg; Ref.No. 2021-300121-WF).
20 The COVID-Hep.net and SECURE-Liver registries data were deemed not to constitute
21 human research by Clinical Trials and Research Governance at the University of Oxford
22 (https://covid-hep.net/img/CTRG_COVID-Hep_20200402.pdf) and by the Institutional
23 Review Board of University of North Carolina (<https://covidcirrhosis.web.unc.edu/faq/>)
24 respectively. The study involving patients from the VOCAL cohort was performed with

1 informed consent and ethical approval from the Miami VA Institutional Review Board (Unique
2 study approval ID 1477437-22).

3

4 **10x single cell RNA sequencing, data analysis and availability**

5 We used our previously published single cell RNA sequencing (scRNAseq) dataset including
6 primary cholangiocytes, cholangiocyte organoids originating from different regions of the
7 biliary tree (intrahepatic ducts, common bile duct and gallbladder), and the same organoids
8 following bile treatment. Tissue dissociation, cell isolation, 10X single cell library preparation
9 and 10X data processing, normalisation and analysis was performed as previously
10 described¹⁴. 10X raw data (fastq files) have been deposited in the repository ArrayExpress
11 with the accession number E-MTAB-8495. Single cell RNA sequencing data were analysed
12 using Anaconda-Navigator 1.9.12, Jupyter Notebook 6.0.3 and Rstudio (version 1.1.463).

13

14 **Human tissue collection and processing**

15 Human primary tissue was obtained from biopsies, deceased transplant organ donors or liver
16 explants after obtaining informed consent. Depending on the application, primary fresh tissue
17 was embedded in OCT (Optimal Cutting Temperature) compound and stored at -80°C; or
18 fixed in 10% formalin, dehydrated and embedded in paraffin. Sections from embedded tissue
19 were cut at a thickness of 5-10 µm using a cryostat or a microtome and mounted on
20 microscopy slides for further analysis.

21

1 **Bile sample collection and processing**

2 Human bile was collected during ERCP (Endoscopic Retrograde Cholangio-
3 Pancreatography) or intraoperatively with informed consent from the patient. For viral RNA
4 quantification samples were immediately lysed using an equal volume of RNA lysis buffer
5 (Sigma) and stored at -20°C.

6 7 **Cell culture**

8 Primary cholangiocytes were isolated and cholangiocyte organoids were derived and
9 cultured using our established methodology^{14,16,50}. Cholangiocyte organoids obtained from
10 intrahepatic ducts (IHD), common bile duct (CBD) and gallbladder (GB) tissue were used in
11 this study. Cholangiocytes derived from any of the different regions of the biliary tree (IHD,
12 CBD, GB) acquired a common gallbladder identity when treated with CDCA, as previously
13 reported¹⁴. The experiments described were performed with cholangiocyte organoids derived
14 from all the three regions of the biliary tree (IHD, CBD and GB) and provided congruent
15 results. For consistency, the results shown correspond only to cholangiocyte organoids
16 derived from the gallbladder (gallbladder cholangiocyte organoids – GCOs).

17 Human primary intestinal organoids, derived from terminal ileum biopsies were provided by
18 Simon Buczacki's group. The organoids were derived following a modification of previously
19 described protocols⁵¹, embedded in Matrigel and cultured in Intesticult (StemCell
20 Technologies) supplemented with Penicillin-Streptomycin and Rho kinase inhibitor (Strattech
21 Scientific).

22 Human primary airway organoids were provided by Joo-Hyeon Lee's lab. The organoids were
23 derived and cultured as previously described²⁴.

1 Vero E6 cells (ATCC™ CRL – 1586), HEK293 cells (ATCC™ CRL – 1573) and HEK293T
2 cells (ATCC™ CRL – 3216) were grown on tissue culture plates or T25 flasks in 10% FBS
3 DMEM supplemented with L-glutamine and Penicillin-streptomycin as previously described⁵².

4

5 **Biological materials availability**

6 Detailed protocols for the derivation of primary organoids have been previously reported^{24,50}.

7 Cell lines are available from standard commercial sources ([https://www.lgcstandards-
8 atcc.org](https://www.lgcstandards-atcc.org) - Vero E6 cells, ATCC™ CRL – 1586; HEK293 cells, ATCC™ CRL – 1573).

9

10 **Modulation of FXR activity**

11 Chenodeoxycholic acid (CDCA) and ursodeoxycholic acid (UDCA) were purchased from
12 Sigma Aldrich (C9377-5G and U-5127-5G), while Z-Guggulsterone (ZGG) was purchased
13 from Santa Cruz (sc-204414) and reconstituted following the manufacturer's instructions. To
14 modulate FXR activity, organoids were incubated with a final concentration of 10 μM CDCA;
15 or 10 μM CDCA in combination with 10 μM of UDCA or ZGG.

16

17 **FXR knock-down**

18 FXR knock-down was performed in cholangiocyte organoids using commercially available
19 lentiviral particles carrying shRNA gene silencer sequences against the human FXR (*NR1H4*)
20 transcript (Santa Cruz; sc-38848-V). Commercially available lentiviral particles carrying
21 control (scrambled) shRNA sequences (Santa Cruz; sc-108080) were used as control.
22 Successfully transduced cholangiocyte organoids were selected with puromycin 24 hours
23 after viral transduction. Quantification of FXR, ACE2 and SHP expression and SARS-CoV-2
24 infection were performed 10 days after FXR knock-down.

25

1 **Chromatin immunoprecipitation**

2 Approximately 6×10^6 cells were used for each chromatin immunoprecipitation (ChIP), and
3 cells were incubated with fresh medium with 100 μ M of CDCA, UDCA or ZGG 2 h before
4 collection. ChIP was performed using the True Micro ChiP kit (Diagenode C01010130)
5 according to manufacturer's instructions. In brief, following pre-clearing, the lysate was
6 incubated overnight with the FXR antibody (Santa Cruz sc-25309 X) (Supplementary Table
7 S1) or non-immune IgG. ChIP was completed and immunoprecipitated DNA was purified
8 using MicroChip DiaPure columns (Diagenode C03040001). Samples were analysed by
9 QPCR using the $\Delta\Delta C_t$ approach as previously described⁵⁰ (see Supplementary Table S3 for
10 primer sequences). Primers flanking the FXR responsive element (FXR RE) on the well-
11 known FXR target gene *OST α* ⁵³ were used as positive control, while primers flanking a site
12 distant from the FXR RE on the ACE2 promoter were used and a negative control. The results
13 were normalized to the enrichment observed with non-immune IgG ChIP controls.

15 **Luciferase reporter**

16 Two different fragments containing the FXRE IR-1 in the ACE2 gene and in the SHP gene
17 were amplified using human genomic DNA as template and inserted onto pGL3-promoter
18 luciferase vector. The ACE2 and SHP IR-1 mutants were generated using a site-directed
19 mutagenesis approach (New England BioLabs E0554S). Sequences of primers used are
20 reported in Supplementary Table S4. These gene reporter constructs were co-transfected
21 with a commercially available FXR expression plasmid (OriGene, SC329876) into HEK293
22 cells using TransIT-293 Transfection Reagent (MirusBio). 24 h after transfection, cells were
23 treated with 50 μ M of CDCA, UDCA and ZGG in fresh media for 8 hours. Luciferase activity
24 was determined with GLO-Luciferase Reporter Assay System (Promega, Madison, ONE-
25 Glo™ Luciferase Assay System) and values were normalized to the empty pGL3 vector.

1
2
3
4
5
6
7
8
9
10
11
12
13
14
15
16
17
18
19
20
21
22
23
24
25

Immunofluorescence, RNA extraction and QPCR

Immunofluorescence, RNA extraction and quantitative real-time PCR (QPCR) were performed as previously described^{65,67,70,71}. A complete list of the primary and secondary antibodies used is provided in Supplementary Table S1. A complete list of the primers used is provided in Supplementary Table S2.

All QPCR data were obtained using a QuantStudio 5 384 Well Block (Thermo Fisher). All QPCR data are presented as the median, interquartile range (IQR) and range (minimum to maximum) of four independent experiments unless otherwise stated. Values are relative to the housekeeping gene Hydroxymethylbilane Synthase (*HMBS*) or Glyceraldehyde-3-Phosphate Dehydrogenase (*GAPDH*). Statistical analysis is described in the relevant section. For comparative immunofluorescence images, the cells or sections being compared were stained simultaneously, using the same primary and secondary antibody master mix. All immunofluorescence images were acquired using a Zeiss LSM 700 or 710 confocal microscope using ZEN 2011 SP7 (Zeiss). The same laser power and exposure settings were used to acquire comparative images. Imagej 2.0.0-rc-69/1.53f software (Wayne Rasband, NIH, USA, <http://imagej.nih.gov/ij>) was used for image processing. Each immunofluorescence image is representative of at least 3 different experiments.

Flow cytometry analyses

Flow cytometry in organoids was performed as previously described⁵⁰. In summary, organoids were collected using Cell Recovery Solution (Corning) for 20 min at 4 °C and were then centrifuged at 444g for 4 min and dissociated to single cells using StemPro Accutase (Invitrogen). Cells were subsequently fixed using 4% paraformaldehyde (PFA) for 20 min at 4 °C. All flow cytometric analyses were performed on a BD LSR-II flow cytometer (BD

1 Biosciences) using BD FACS Diva 8.0.3 (BD Bioscience) and analysed using FlowJo
2 v.10.4.2. The gating strategy is provided in Supplementary Figure S1.

3

4 **Dose-response curves for ACE2**

5 Primary organoids were treated with 0.01 μM – 1 mM of CDCA, UDCA or ZGG and ACE2
6 expression was measured via QPCR. The inhibitory effect of UDCA and ZGG on FXR
7 activation was assessed on cells treated with 10 μM of CDCA. Data were analysed using the
8 Sigmoidal, 4PL, X is log(concentration) function in GraphPad Prism.

9

10 **Cytotoxicity and viability**

11 Primary organoids were treated with 0.1 μM – 100 μM of CDCA, UDCA or ZGG and the
12 percentage of viable cells were counted using trypan blue and a Countess II cell counter
13 (ThermoFisher). Cellular viability in primary organoids treated with 10 μM of CDCA, UDCA
14 or ZGG was measured using the resazurin-based assay PrestoBlue (Invitrogen, A13261)
15 using SoftMax Pro 5.4.4 on a SpectraMax M2 (Molecular Devices)..

16

17 **SARS-CoV-2 isolate**

18 The SARS-CoV-2 virus used in this study are the clinical isolate named "SARS-CoV-
19 2/human/Liverpool/REMRQ0001/2020"⁵² derived from a patient's naso-pharyngeal swab and
20 isolated by Lance Turtle (University of Liverpool) and David Matthews and Andrew Davidson
21 (University of Bristol) and the delta lineage (B.1.617.2) hCoV-19/England/SHEF-
22 10E8F3B/2021 (G|SA|D accession number EP|_|SL_1731019) kindly provided by Professor
23 Wendy Barclay, Imperial College London, London, UK through the Genotype to Phenotype
24 National Virology Consortium (G2P-UK).

25

1 **SARS-CoV-2 infection**

2 All work with infectious SARS-CoV-2 was performed under containment level 3 (CL-3)
3 conditions either at the Cambridge institute of Therapeutic Immunology and Infectious
4 Diseases (CITIID) or at the Centre for Excellence and Long-acting Therapeutics (CELT).
5 SARS-CoV-2 was gifted to the users of the CITIID CL-3 by Ian Goodfellow^{54,55} and
6 propagated on Vero E6 cells as previously described⁵². Viral titration was determined using
7 the TCID₅₀ method on Vero E6 cells⁵². For viral infection primary organoids were passaged
8 and incubated with SARS-CoV-2 in suspension at a multiplicity of infection (MOI) of 1 for 2
9 hours. Subsequently, the infected organoids were washed twice with 10 ml of culture media
10 to remove the viral particles. Washed organoids were plated in 40 µl Matrigel domes, cultured
11 in organoid medium and harvested at different timepoints.

12 To test whether SARS-CoV-2 produced by infected COs retained its infective capacity, the
13 supernatant from infected COs was collected at 24 hours post infection and used to infect a
14 fresh batch of SARS-CoV-2 naive organoids.

15

16 **Fixation of SARS-CoV-2 infected organoids/tissue**

17 Organoids for IF were cultured on coverslips, placed at the bottom of the wells of a 24-well
18 plate. The culture medium was aspirated and replaced with 500 µl of 8% PFA for a minimum
19 of 30 minutes. Following fixation, the coverslips were recovered, transferred to a clean plate,
20 and fresh PBS was added. Primary tissue was fixed for a minimum of 4 hours with 8% PFA
21 and then transferred to a clean plate with fresh PBS.

22

23 **Quantification of viral infection**

24 Organoids or primary tissue were infected in 24-well plates as described above. Total RNA
25 samples were prepared by adding 500 µl of lysis buffer (25 mM Tris-HCL+ 4 M Guanidine

1 thiocyanate with 0.5% β -mercaptoethanol) to each well and transferring the lysate (1 ml) to a
2 5 ml Eppendorf tube. Tubes were vortexed, and 100% analytical grade ethanol was added
3 to a final concentration of 50%. After 10 minutes of incubation, 860 μ l of lysis buffer
4 (containing MS2 bacteriophage as an internal extraction and amplification control) were
5 added and thoroughly mixed. The RNA was then isolated using an RNA spin column as
6 previously described⁵⁶. Viral replication was quantified using QPCR for the expression of the
7 viral RNA-dependent RNA polymerase (*RdRp*) gene with primers specific for a 222 bp long
8 fragment from a conserved region of the gene. *GAPDH* was used as a housekeeping gene
9 and MS2 was used as an internal reference as previously described⁵⁶. Viral load was
10 determined relative to *GAPDH*. The sequences of primers/probes used are provided in
11 Supplementary Table S2.

12

13 **Transmission Electron Microscopy**

14 Infected organoids were fixed in 4% paraformaldehyde; 2.5% glutaraldehyde in 0.1M sodium
15 cacodylate buffer overnight at 4°C, washed and stored in 0.1M sodium cacodylate buffer
16 before processing. Samples were postfixed in 1% aqueous osmium tetroxide (TAAB, UK);
17 1.5% potassium ferricyanide overnight at 4°C, washed thoroughly in dH₂O and *en*
18 *bloc* stained in 3% aqueous uranyl acetate (Agar Scientific, UK) for 24h at 4°C. Samples were
19 dehydrated through an ethanol series, infiltrated with 1:1 propylene oxide:resin (TAAB, UK)
20 and blocks of fresh resin polymerised at 60°C for 48h. Ultrathin sections of ~60nm were cut
21 from blocks using an EM UC7 ultramicrotome (Leica Microsystems, UK) and mounted on
22 copper grids coated with carbon and formvar (Agar Scientific, UK). Grids were post-stained
23 in uranyl acetate and lead citrate, imaged using a HT7800 transmission electron microscope
24 (Hitachi High Technologies, Japan) operating at 100kV and acquired using HT7800 TEM
25 operating software version 01.21 (Hitachi).

1

2 **HEK293 cells stably expressing ACE2**

3 HEK293T cells stably expressing ACE2 were generated as previously described⁵⁷. Briefly,
4 HEK293T cells transduced with ACE2 under the control of the spleen focus-forming virus
5 (SFFV) promoter were sorted for high cell-surface ACE2 expression and single-cell cloned.
6 Following expansion, a clone with stable, homogeneously high expression of ACE2 was
7 selected via FACS.

8

9 **Luciferase reporter for SARS-CoV-2 replication**

10 A luciferase reporter for SARS-CoV-2 protease activity during viral replication was generated
11 as previously described⁵⁷. In brief, HEK293T reporter cells stably expressing ACE2, Renilla
12 luciferase (Rluc) and SARS-CoV-2 Papain-like protease-activatable circularly permuted
13 firefly luciferase (FFluc) were seeded in flat-bottomed 96-well plates. The following morning,
14 cells were treated with the indicated doses of CDCA, UDCA and ZGG, and infected with
15 SARS-CoV-2 at a MOI of 0.01. The SARS-CoV-2 RdRp inhibitor remdesivir and a neutralising
16 antibody cocktail blocking the interaction between SARS-CoV-2 spike and ACE2 (REGN-
17 COV2) were included as positive controls. After 24 hours, cells were lysed in Dual-Glo
18 Luciferase Buffer (Promega, E2920) diluted 1:1 with PBS and 1% NP-40. Lysates were then
19 transferred to opaque 96-well plates, and viral replication quantitated as the ratio of
20 FFluc/Rluc activity measured using the Dual-Glo kit (Promega) according to the
21 manufacturer's instructions. FFluc/Rluc ratios were expressed as fraction of maximum, then
22 analysed using the Sigmoidal, 4PL, X is log(concentration) function in GraphPad Prism.

23

24 **Animal study**

1 *Mice*: the experiments were performed in accordance with the Animal Research: Reporting
2 of In Vivo Experiments (ARRIVE) guidelines and approved by the Animal Ethics Committee
3 of the Medical University of Vienna and the Federal Ministry of Science, Research and
4 Economy (BMFWF-66.009/0008-WF/3b/2015). Friend Virus B NIH (FVB/N) mice were bred
5 in house. Animals were housed in a 12 hours/12 hours dark/light cycle, with a humidity of 45-
6 65% and temperature of 20-24°C. Chow was obtained from SAFE—Scientific Animal Food
7 & Engineering (product number A04). Age matched female animals were used. Animals were
8 assigned randomly to treatment and control groups. Animals in the treatment group received
9 chow supplemented with 1% w/w UDCA and 1%w/w cholic acid (CA), while animals in the
10 control group received chow supplemented with 1% w/w cholic acid (CA)⁵⁸. Cholic acid was
11 used to activate FXR and study the impact of UDCA on FXR activation¹⁹. The animals were
12 fed ad libitum for 7 days. Data were analysed blinded to the identity of the experimental
13 groups.

14 *Hamsters*: the experiments were performed in accordance with the UK Home Office Animals
15 Scientific Procedures Act (ASPA, 1986). Additionally, all studies were approved by the
16 University of Liverpool Animal Welfare and Ethical Review Board and performed under UK
17 Home Office licences PP9284915 and PP4715265. Golden Syrian Hamsters were purchased
18 from Janvier Labs, France. Animals were housed in a 12 hours/12 hours dark/light cycle, with
19 a humidity of 45-65% and temperature of 20-24°C. Age matched male animals were used
20 weighing between 80 – 100g. Animals were assigned randomly to treatment and control
21 groups. Animals in the treatment groups received a daily oral regimen of UDCA (416 mg/kg)
22 by oral gavage while animals in the control group received vehicle only. The animals were
23 fed ad libitum and treatment continued for 7 days to achieve similar blood concentration of
24 UDCA observed in patients taking UDCA (Extended Data Fig. 9a)²⁸.

1 For testing UDCA intervention against SARS-CoV-2 infection, one hamster was directly
2 inoculated by the intranasal route with 1×10^2 PFU/hamster in 100 μ l of PBS. Each infected
3 hamster was placed on one side of a transmission cage. The cage was divided with an
4 aerated barrier allowing the infected hamster to be co-housed with previously treated
5 uninfected animals housed on the other side permitting to study viral infection by aerosol
6 transmission. Daily swabs were collected from all animals to monitor the infection via QPCR
7 for the viral N gene. On day 4 post infection the hamsters were euthanised and lungs and
8 nasal turbinates were collected for quantification of viral infection. The experiment was
9 repeated n=3 times for a total of n=9 UDCA animals and n=6 vehicle animals. Data were
10 analysed blinded to the identity of the experimental groups.

11

12 **Quantification of UDCA concentration**

13 UDCA was quantified from hamster plasma using a LCMS assay that was validated using
14 FDA industry guidelines. Quantification was achieved via LC-MS/MS (6500+ QTRAP,
15 SCIEX) operating in negative mode. UDCA was detected using MRM where the following
16 ions were monitored for quantification: UDCA (m/z 391 > 391 and internal standard
17 mefloquine 379.1>320.1). A stock solution of 1 mg/ml UDCA was prepared in methanol and
18 stored at 4°C until use. A standard curve was prepared in plasma by serial dilution from 40000
19 ng/mL to 312.5 ng/mL and an additional blank solution was also used. Chromatographic
20 separation was achieved using a multi-step gradient with a Acquity BEH C18 column (2.1mm
21 x 100mm 1.7 μ m; Waters, Wilmslow, UK) using mobile phases A (100% water, 0.1% formic
22 acid and 5mM ammonium formate) and B (90% acetonitrile 10% methanol, 0.1% formic acid
23 and 5mM ammonium formate). Chromatography was conducted over 3.5 minutes. At the
24 start of each run, mobile phase A was 80% until 0.5 minutes when mobile phase B was
25 increased to 47% over 0.5 minutes. Mobile phase B was then increased over 1 minute to

1 51%. Mobile phase B was then increased to 100% at 2.5 minutes which was held until 3
2 minutes. Mobile phase B was reduced to 20% and held till 3.5 minutes. Samples were
3 extracted from hamster plasma via protein precipitation. Briefly, 100µl of standard, QC, blank
4 plasma, or study sample were treated with 400µl of ACN. Samples were then vortexed
5 followed by centrifugation at 3500rpm for 5 minutes. 400µl of supernatant was transferred to
6 fresh glass vials and evaporated under a steady stream of nitrogen. Samples were
7 reconstituted in 50:50 water methanol and analysed. Inter- and intra- assay variance was
8 assessed by 3 levels of independent quality controls. Coefficient of variation of accuracy and
9 precision were <15% in all assays.

10

11 ***Ex situ* normothermic perfusion (ESNP) of human lungs**

12 For the *ex situ* perfusion of a single pair of human lungs, two bespoke ESNP circuits
13 (Medtronic, Ireland) were used. In brief, this circuit facilitates pressure monitored perfusion
14 with normothermic perfusion solution consisting of bovine serum albumin (BSA) (70 g/l),
15 dextran 40 (5 g/l), modified Krebs Henseleit buffer (9.2 g/l), sodium bicarbonate solution (28
16 ml/l), calcium chloride (25 ml/l) and heparin (3750 units/l). The pair of human lungs used,
17 were perfused following the physiological principles previously described⁵⁹.

18 *Lung ESNP experimental setup*

19 The experiment shown in Fig. 3 was performed on a pair of lungs declined for clinical lung
20 transplantation due to the donor's past medical history. The left and the right lungs were
21 divided at the carina and common pulmonary artery bifurcation. For each isolated lung, the
22 pulmonary artery and the pulmonary vein were cannulated and an endobronchial tube was
23 inserted into the main bronchus. The cannulae of each lung were connected to an entirely
24 independent ESNP circuit (control and experimental lung circuits). The endobronchial tube
25 of each lung was connected to an independent mechanical ventilator (Drägerwerk AG & Co.

1 KGaA, Germany). Mechanical ventilation was performed using room air with a positive end
2 expiratory pressure of 5 mmHg, target tidal volume of 130 ml at 5 bpm for the left lung and
3 140 ml at 6 bpm for the right lung.

4 *Timing and duration of ESNP*

5 Perfusion started simultaneously for both lungs. After 30 minutes of stable perfusion,
6 UDCA/carrier was administered and this time point was defined as 0 hours (0h). ESNP was
7 performed for 6 hours for both lungs after administration of UDCA/carrier. The end of
8 experiment timepoint is defined as 6 hours (6h).

9 *Experimental timepoints and sample collection*

10 Baseline tissue and perfusate samples were collected simultaneously from both lungs before
11 UDCA/carrier administration. We defined these samples as 0h samples. Corresponding
12 samples were collected simultaneously from each lung at the end of the experiment at 6h.
13 We defined those as 6h samples.

14 The following samples were collected from each lung per timepoint: n=4 independent lung
15 biopsies, n=4 surgically excised independent samples from the pulmonary artery, n=4
16 surgically excised independent samples from the main bronchus, and n=4 independent
17 samples from the perfusate in each circuit. The independent tissue samples refer to different
18 locations of the organ. Biopsies were surgically excised and the lung parenchymal samples
19 from 0h were taken from peripheral areas separated from the remaining lung by staples
20 (Medtronic, Ireland) to seal the defect. 6h samples were taken using the same approach.
21 Please also refer to the results section 'UDCA limits SARS-CoV-2 infection in human organs
22 *ex vivo*'.

23 24 ***Ex situ* normothermic perfusion (ESNP) of donor livers**

1 The OrganOx metra normothermic liver perfusion device was used for *ex situ* perfusion of
2 human livers as previously described^{14,29,31}. The machine, which is clinically used for
3 preservation of livers for transplantation enables prolonged automated organ preservation by
4 perfusing it with ABO-blood group-matched normothermic oxygenated blood. The perfusion
5 device incorporates online blood gas measurement, as well as software-controlled algorithms
6 to maintain pH, PO₂ and PCO₂ (within physiological limits), temperature, mean arterial
7 pressure and inferior vena cava pressure within physiological normal limits.

8 *Experimental setup*

9 2 donor livers not used for transplantation were maintained with ESNP. In brief, the hepatic
10 artery, portal vein, inferior vena cava and bile duct were cannulated, connected to the device
11 and perfusion commenced. One liver was randomly chosen to receive a solution of UDCA
12 dissolved in 0.9% NaCl (experimental liver), while the other liver (control) was chosen to
13 receive the same volume of carrier (0.9% NaCl). UDCA was resuspended in 0.9% (w/v) NaCl
14 solution and injected in the blood circuit to achieve a final concentration of 2000 ng/ml, which
15 is the steady state concentration of UDCA detected in serum after multiple doses of UDCA²⁸.

16 *Timing and duration of ESNP*

17 The time of UDCA/carrier administration following the start of ESNP was defined as 0 hours
18 (0h). ESNP was performed for 12 hours for both livers after administration of UDCA/carrier.
19 The end of experiment timepoint is defined as 12 hours (12h).

20 *Experimental timepoints and sample collection*

21 Baseline tissue and perfusate samples were collected from each liver before UDCA/carrier
22 administration. We defined these samples as 0h samples. Corresponding samples were
23 collected from each liver at the end of the experiment at 12h. We defined those as 12h
24 samples.

1 The following samples were collected from each liver per timepoint: n=4 independent
2 surgically excised gallbladder samples, n=4 independent liver biopsies, and n=4 independent
3 samples from the circulating perfusate. Independent gallbladder samples and liver biopsies
4 were obtained from different locations of the organ. Gallbladder samples were surgically
5 excised and the gallbladder wall was sutured to close the defect.

6

7 ***Ex vivo* SARS-CoV-2 infection of human tissue**

8 The infection of human tissue maintained *ex vivo* with SARS-CoV-2 occurred in a CL-3 facility
9 following the ESNP experiment. 4 independent samples from the lung parenchyma, bronchi
10 and the vasculature (pulmonary artery) of each lung were collected per timepoint, i.e. at the
11 start of the ESNP experiment (0h) and at the end (6 hours) of the lung perfusion. 4
12 independent samples from each ESNP liver gallbladder were collected per timepoint, i.e. at
13 the start of the ESNP experiment (0h) and at the end (12 hours) of the liver perfusion. Sample
14 collection was performed as described in the section '*Ex situ* normothermic perfusion (ESNP)
15 of donor livers'.

16 The freshly obtained lung, bronchial, vascular and gallbladder tissues were processed into
17 small rectangular pieces of 0.5x0.5 cm and were rinsed with University of Wisconsin solution
18 (lung, bronchial and vascular tissues) or William's E medium with supplements as previously
19 described⁵⁰ (gallbladder tissue). Washed specimens were placed in wells of a 24-well plate
20 (one specimen per well) and infected with SARS-CoV-2. An inoculum of 1.2×10^5 PFU/ml at
21 500 μ l per well was used. After two hours, the inoculum was removed, and the specimens
22 were washed three times with PBS. The infected human tissue was then cultured in 500 μ l
23 of advanced DMEM with supplements⁶⁰ (lung, bronchial and vascular tissues) or William's E
24 medium with supplements (gallbladder tissue). Supernatant and tissue were harvested for
25 QPCR and immunofluorescence at 2 and 24 hours post infection.

1
2
3
4
5
6
7
8
9
10
11
12
13
14
15
16
17
18
19
20
21
22
23
24
25

Blood sample collection and processing

Blood samples were collected from patients as part of the UK-PBC Nested Cohort study after obtaining informed consent, anonymised and analysed by a blinded researcher. To obtain serum from full blood, the samples were spun at 4°C at 1000 g for 10 minutes to allow for serum separation and serum was collected as the supernatant. All blood samples were collected after fasting.

ACE2 enzymatic activity

ACE2 enzymatic activity was performed on serum samples and tissue lysates using the ACE2 activity fluorometric kit (abcam ab273297) following manufacturer's instructions using SoftMax Pro 5.4.4 on a SpectraMax M2 (Molecular Devices).

ACE2 measurement in nasal epithelial cells of volunteers

Recruitment

Following approval by local ethics committee (Ethik-Kommission der Ärztekammer Hamburg; Ref.No. 2021-300121-WF), the study was advertised in the University Medical Centre Hamburg-Eppendorf amongst clinicians regularly prescribing UDCA, and thus familiar with the drug and its possible side-effects. 8 clinicians who volunteered to participate in the study were recruited following informed consent. The characteristics of the volunteers are provided in Supplementary Table S5.

Study design and exclusion criteria

UDCA was self-administered at the clinically approved dose of 15mg/kg/day in a single morning dose for 5 days. Nasal epithelium samples for ACE2 measurement were collected each morning prior to UDCA administration using the Citoswab nasopharyngeal swab

1 collection kit (Corona Smear). Day 0 samples were collected before the first UDCA dose.
2 Daily morning samples were collected during UDCA treatment (days 1-5). Following drug
3 washout, repeat nasopharyngeal swabs were collected between days 22 and 28. Volunteers
4 providing samples with no detectable RNA were excluded from the study.

5 *ACE2 measurement*

6 RNA was extracted from the Citoswab nasopharyngeal swab collection kit (Corona Smear)
7 using the RNeasy micro kit (Qiagen) according to the manufacturer's instructions. ACE2
8 mRNA levels were measured using QPCR (see Immunofluorescence, RNA extraction and
9 QPCR section). The results are shown as fold change over the housekeeping gene GAPDH.
10

10

11 **Serum proteome analysis in patients with primary biliary cholangitis (PBC)**

12 Serum proteomic analysis was performed in the UK-PBC patient cohort as described in
13 Barron-Millar, *et al.*³². Blood samples were obtained with informed consent and appropriate
14 ethical approval (UK-PBC tissue bioresource, 14/NW/1146). Serum samples were assayed
15 using the Olink proteomics™ platform (www.olink.com).
16

16

17 **Patient data**

18 Data for patients with chronic liver disease were collected as described elsewhere^{34,61}.
19 Briefly, collated results from two open online reporting registries (COVID-Hep.net and
20 SECURE-Liver) were examined. Reports were asked to report cases of laboratory confirmed
21 COVID-19 in patients with chronic liver disease at the end of the disease course. Anonymous
22 clinical and demographic data were collected, filtered to remove duplicate entries, those with
23 incomplete records, those with prior liver transplantation, those not over 18 years of age,
24 those over 90 years of age, and those without laboratory confirmed infection.

1 Data for patients with liver transplant were collected as described elsewhere³⁵. Briefly, data
2 from patients with a liver transplant who were alive on the 1st of March 2020 were examined.
3 Participants who had no COVID-19 infection, were unvaccinated or developed COVID-19
4 within 30 days from their first UDCA prescription were excluded. The resulting study sample
5 included n=24 patients on UDCA and 95 who were not on UDCA and was used for the
6 analysis.

8 **Statistical analyses**

9 Statistical analyses were performed using Microsoft Excel v 16.19, Rstudio (version 1.1.463),
10 GraphPad Prism 9 or Stata 15.1 (StataCorp, College Station, TX, USA). The normal
11 distribution of our values was evaluated using the Shapiro-Wilk test where appropriate. For
12 comparison between two groups, a two-tailed Student's t-test or the non-parametric Mann-
13 Whitney test were used depending on the normality of our distribution. To compare matched
14 samples from the same individual a two-tailed paired Student's t-test was used (the normal
15 distribution of our data was confirmed using the Shapiro-Wilk test). Variance between
16 samples was tested using the Brown-Forsythe test. For comparing multiple groups to a
17 reference group one-way ANOVA followed by Dunnett's test was used between groups with
18 equal variance. Immunofluorescence images are representative of 4 independent
19 experiments. Data are represented in box plots and elements are defined as follow: center
20 line, median; box, interquartile range (IQR); whiskers, range; error bars, standard deviation.
21 Serum proteomic analysis was performed using Rstudio (version 1.1.463). The correlation
22 between ACE2 levels and UDCA administration was interrogated using multiple linear
23 regression analysis with the *lm* function in R. ACE2 expression data was defined as the
24 independent variable, while UDCA administration, sex, age, body mass index (BMI), stage of

1 chronic liver disease according to the Child-Turcotte-Pugh class and alkaline phosphatase,
2 were defined as dependent variables.

3 COVID-Hep and SECURE-Liver data (exploratory cohort): for propensity score-matched
4 analyses, 1:5 matched samples (using the nearest neighbour approach) were constructed
5 with hospitalisation, physician-reported requirement for intensive care, intensive care
6 admission, mechanical ventilation, and death as the outcome variables. Covariables used
7 were age, sex and categorical stage of chronic liver disease according to the *Child-Turcotte-*
8 *Pugh* class, diabetes, chronic pulmonary disease (COPD/asthma), immunosuppressive
9 therapy, increased BMI (BMI>25), and the presence of non-alcoholic fatty liver disease, due
10 to its association with increased COVID19 risk. Importantly, alcohol-related liver disease
11 (ARLD) is also associated with increased COVID19 risk; however, patients could not be
12 propensity scored matched between the 2 cohorts, as there were no patients with ARLD
13 receiving UDCA. Consequently, patients with ARLD were excluded.

14 VOCAL data (validation cohort): for propensity score-matched analyses, 1:3 matched
15 samples (using a Greedy matching algorithm) were constructed with moderate/severe/critical
16 COVID-19 and severe/critical COVID-19 according to the NIH severity scale as the outcome
17 variables. Covariables used were age, sex, ethnicity, location within the United States,
18 diabetes, BMI, COPD, type of immunosuppressive therapy (calcineurin Inhibitor with or
19 without anti-metabolite therapy) and dominant SARS-CoV-2 variant.

20 Propensity score matching was performed using the *teffects* function in Stata. The average
21 treatment effect on the treated (ATET) was calculated with robust Abadie-Imbens standard
22 errors and derived 95% confidence intervals are presented.

23

1 **Data availability:** Single-cell RNA sequencing data are available on ArrayExpress.
2 Accession number: E-MTAB-8495. Source data for in vivo experiments and relative to
3 Extended Data Figure 10 are provided.
4

5 **Acknowledgements:** The authors would like to thank the European Association for the
6 Study of the Liver (EASL) and the American Association for the Study of Liver Disease
7 (AASLD) for supporting the COVID-Hep and SECURE-Liver registries; Prof Stefan Marciniak
8 and Prof Paul J. Lehner for comments and feedback on the manuscript; Prof Ian Goodfellow
9 for providing the viral isolate; Dr. Mark Wills and Dr. Simon Clare for all their work ensuring a
10 safe CL3 working environment; Claire Cormie for general lab support; the NIHR Cambridge
11 BRC Cell Phenotyping Hub for their help with flow cytometry and processing of samples; the
12 building staff of the Jeffrey Cheah Biomedical Centre for maintaining the institute open and
13 safe during the period of lockdown; Katja Füssel for coordinating the volunteer study and
14 sample collection at the University Medical Centre Hamburg-Eppendorf; Janeane Hails,
15 Konstantina-Irene Nikitopoulou and Abigail Ford for collecting blood samples; Maria Colzani
16 for advising on flow cytometry; Anne Wiblin from Abcam for advising on antibodies; the
17 Cambridge Biorepository for Translational Medicine for the provision of human tissue used
18 in the study.
19

20 **Funding:** T.B. was supported by an EASL Juan Rodès PhD fellowship. F.S. was supported
21 by a UKRI Future Leaders fellowship, the Evelyn trust, an NIHR Clinical Lectureship, the
22 Academy of Medical Sciences Starter Grant for Clinical Lecturers, the Addenbrooke's
23 Charitable Trust and the Rosetrees Trust. Additional, the F.S. lab is supported by the
24 Cambridge University Hospitals National Institute for Health Research Biomedical Research
25 Centre and the core support grant from the Wellcome Trust and Medical Research Council

1 (MRC) of the Wellcome–Medical Research Council Cambridge Stem Cell Institute. The L.V.
2 lab is funded by the ERC advanced grant New-Chol, the Cambridge University Hospitals
3 National Institute for Health Research Biomedical Research Centre and the core support
4 grant from the Wellcome Trust and Medical Research Council (MRC) of the Wellcome–
5 Medical Research Council Cambridge Stem Cell Institute. M.M., S.F. and G.D. are funded by
6 the NIHR Cambridge Biomedical Research Centre and NIHR AMR Research Capital
7 Funding Scheme [NIHR200640]. The views expressed are those of the author(s) and not
8 necessarily those of the NIHR or the Department of Health and Social Care. V.L.M. was
9 funded by an MRC Clinical Research Training Fellowship. G.F.M. was funded by a post-
10 doctoral fellowship from the National Institute for Health Research (NIHR) Rare Diseases –
11 Translational Research Collaboration (RD-TRC) and by an MRC Clinical Academic Research
12 Partnership (CARP) award. The UK-PBC Nested Cohort study was funded by an MRC
13 Stratified Medicine award (MR/L001489/1). C. J. R. I. was supported by the Medical
14 Research Council (MC_UU_12014). T.M. is funded via a Wellcome Trust Clinical Research
15 Training Fellowship (102176/B/13/Z). The Davenport lab was supported by BHF
16 TG/18/4/33770, Wellcome Trust 203814/Z/16/A, Addenbrooke’s Charitable Trust. The
17 COVID-Hep.net registry was supported by the European Association for the Study of the
18 Liver (EASL) and the SECURE-Liver registry was supported by the American Association for
19 the Study of Liver Disease (AASLD). Lung perfusion experiment was supported by the
20 National Institute for Health Research Blood and Transplant Research Unit (NIHR BTRU) in
21 Organ Donation and Transplantation at Newcastle University and the University of
22 Cambridge in partnership with NHS Blood and Transplant (NHSBT). The views expressed
23 are those of the author(s) and not necessarily those of the NIHR, the Department of Health
24 and Social Care or NHSBT. K. F. is funded by the YAEL foundation. G. B. is funded by the
25 European Reference Network for Hepatological Diseases (ERN RARE LIVER). A.O.

1 acknowledges funding for preclinical research on treatment and prevention of COVID19 from
2 Unitaid (2020-38-LONGEVITY) the Engineering and Physical Sciences Research Council
3 (EPSRC; EP/R024804/1), the Wellcome Trust (222489/Z/21/Z) and UK Research and
4 Innovation (UKRI; BB/W010801/1). N. J. M. acknowledges funding from the MRC (CSF ref.
5 MR/P008801/1 to N.J.M.), NHSBT (grant ref. WPA15-02 to N.J.M.), Addenbrooke's
6 Charitable Trust (grant ref. to 900239 N.J.M.).

7
8 **Author contributions:** T.B. conceived and designed the study, performed experiments,
9 acquired, interpreted and analysed the data, developed and validated the protocols
10 described, generated the figures, wrote and edited the manuscript. M.M. performed SARS-
11 CoV-2 infection experiments, collected and processed infectious samples, contributed to data
12 interpretation and critical revision of the manuscript for important intellectual content. G.J.W.
13 acquired, analysed and interpreted patients' data from the COVID-Hep and SECURE-Liver
14 registries and contributed to critical revision of the manuscript for important intellectual
15 content. B.V.J. acquired, analysed and interpreted patients' data from the COVID-Hep and
16 SECURE-Liver registries and contributed to critical revision of the manuscript for important
17 intellectual content. C.D.F. performed mouse experiments. G.B. contributed to healthy
18 volunteer study. L.W., C.G., M.B. and W.S. established lungs on ESNP and performed the
19 lung ESNP experiment. P.P.G. performed SARS-CoV-2 infection experiments in HEK293T
20 cells and generated the luminescent biosensor. W.T.H.G. contributed to sample collection
21 and critical revision of the manuscript for important intellectual content. S.B. contributed to
22 generation of luciferase reporter. S.D. performed transmission electron microscopy sample
23 processing and preparation. D.M. performed bioinformatic analyses. J.Sh. performed
24 hamster experiments and contributed to critical revision of the manuscript for important
25 intellectual content. M.N., H.B., L.T., J.Her., H.C., C.B., A.V., J.St. and E.K. performed

1 hamster experiments. P.C. and H.P. performed UDCA quantification *in vivo*. S.F. and P.M.
2 contributed to viral infection experiments. S.V., M.D.D. and T.W.M.C. expanded and provided
3 cell lines, contributing to cell culture. V.L.M. contributed to blood sample collection. R.E.K.
4 and T.L.W. provided primary tissue samples. J.A.H. and D.R. contributed to sample
5 processing. V. G., M.V.G and O.C.T. provided samples for QPCR. J.B. provided primary
6 tissue. S.S. and S.S.U. contributed to critical revision of the manuscript for important
7 intellectual content. L.S. and C.F. provided perfusionist support for ESNP experiments. K.S.-
8 P. provided primary tissue and established livers on ESNP. S.E.D. provided primary tissue
9 and contributed to histological analyses. D.C. and P.H. contributed to confocal imaging. A.W.,
10 H.H., E.M. and C.J.R.I. contributed to critical revision of the manuscript for important
11 intellectual content. B.D., D.R.B. and R.D.F. acquired and analyzed patient data included in
12 the VOCAL registry. T.M., E.B., A.M.M. and A.S.B.IV acquired and analyzed patient data
13 included in the COVID-Hep and SECURE-Liver registries. R.K.G., S.B. and V.G.G.
14 contributed to critical revision of the manuscript for important intellectual content. G.C. and
15 A.P.D. provided primary tissue samples and contributed to critical revision of the manuscript
16 for important intellectual content. S.J.A.B. and J-H.L. provided primary organoids, contributed
17 to data interpretation and critical revision of the manuscript for important intellectual content.
18 N.M. supervised the SARS-CoV-2 infection experiments in HEK293T cells, contributed to
19 data interpretation and reviewed the manuscript for important intellectual content. M.T.
20 provided animals and reviewed the manuscript for important intellectual content. A.J.F.
21 provided donor lungs and co-designed the ESNP lung experiment, contributed to ESNP
22 experiments and reviewed the manuscript for important intellectual content. P.G. provided
23 tissue and bile samples and reviewed the manuscript for important intellectual content. A.J.B.
24 and C.J.E.W. provided tissue and bile samples, contributed to ESNP experiments and
25 reviewed the manuscript for important intellectual content. G.F.M. provided samples and

1 contributed to critical revision of the manuscript for important intellectual content and sample
2 provision. G.D. contributed to critical revision of the manuscript for important intellectual
3 content. A.O. led the hamster study, contributed to data interpretation and reviewed the
4 manuscript for important intellectual content. A.W.L. acquired and analysed patient data
5 included in the COVID-Hep and SECURE-Liver registries, performed the volunteer study and
6 contributed to critical revision of the manuscript for important intellectual content. L.V.
7 designed and conceived the study, interpreted the data and edited the manuscript. F.S.
8 designed and conceived the study, interpreted the data, edited the manuscript and performed
9 ESNP experiments. All the authors approved the manuscript.

10

11 **PBC-Research consortium:** George F Mells, please see affiliations^{3,13}.

12

13 **Competing interests:** F.S., L.V. and K.S.-P. are founders and shareholders of Bilitech LTD.
14 L.V. is a founder and shareholder of DEFINIGEN. The remaining authors have no competing
15 interests to disclose.

16

17 **Extended Data Figure legends**

18 **Extended Data Fig. 1. Expression of SARS-CoV-2 entry genes in cholangiocytes. (a)**

19 Schematic illustration of different primary human cholangiocyte populations corresponding to
20 different areas of the biliary tree and cholangiocyte organoids (COs) derived from different
21 areas of the biliary tree grown in absence or presence of the bile acids. **(b)** UMAP plot
22 illustrating different cholangiocyte populations from (a) analysed by scRNAseq. **(c)** UMAP
23 plots showing that viral entry related genes are predominantly expressed in extrahepatic
24 cholangiocytes and COs treated with bile acids. **(d-e)** Immunofluorescence illustrating that
25 ACE2 is expressed in extrahepatic cholangiocytes **(d)** and that SARS-CoV-2 infects

1 gallbladder cholangiocytes of COVID-19+ patient but not intrahepatic cholangiocytes (e). N=4
2 independent samples. Scale bars 50 μ m. (f) QPCR confirming detection of SARS-CoV-2
3 RNA in bile of COVID-19+ patients. Housekeeping gene, HMBS; n=4; two-tailed Mann-
4 Whitney test; centre line, median; box, interquartile range (IQR); whiskers, range; bars,
5 standard deviation. (g) Violin plot of scRNAseq data from (b) showing that cholangiocyte
6 organoids upregulate ACE2 when treated with bile acids regardless of their region of origin.
7 (h) QPCR validating that upon treatment with the bile acid CDCA cholangiocyte organoids
8 assume a gallbladder identity expressing the gallbladder marker SOX17 and upregulating
9 ACE2 at levels comparable to primary gallbladder. Housekeeping gene, HMBS; n=4
10 independent experiments; one-way ANOVA adjusted for multiple comparisons; ns, non-
11 significant; centre line, median; box, interquartile range (IQR); whiskers, range; bars,
12 standard deviation. (i) Immunofluorescence showing that CDCA induces ACE2 expression
13 in gallbladder cholangiocyte organoids (GCOs). N=4 independent experiments. Scale bars
14 50 μ m.

15
16 **Extended Data Fig. 2. CDCA-treated GCOs can be infected by SARS-CoV-2.** (a)
17 Schematic representation of the methodology used to infect GCOs with SARS-CoV-2 and
18 test the capacity of SARS-CoV-2 virions produced in GCOs to infect new (uninfected) cells.
19 (b) Immunofluorescence validating SARS-CoV-2 infection in GCOs. N=4 independent
20 experiments. Scale bars 50 μ m. (c) QPCR confirming infection of CDCA-treated GCOs with
21 SARS-CoV-2 propagated in VERO E6 cells (top panel) and with SARS-CoV-2 propagated in
22 GCOs treated with CDCA (bottom panel), illustrating that SARS-CoV-2 produced in
23 GCOs+CDCA retains its infectious capacity. Scale bars 50 μ m; housekeeping gene, GAPDH;
24 n=4 independent experiments; Kruskal-Wallis test adjusted for multiple comparisons; centre
25 line, median; box, interquartile range (IQR); whiskers, range; bars, standard deviation. (d)

1 QPCR showing up-regulation of innate immune and anti-viral response genes in
2 GCOs+CDCA following SARS-CoV-2 infection. Housekeeping gene, GAPDH; n=4, 2
3 biological and 2 technical replicates; two-tailed Mann-Whitney test (IL-1 β , IL-6, IFN α) and
4 two-tailed unpaired t-test (TNF α , IFN λ). (CDCA concentration, 10 μ M); centre line, median;
5 box, interquartile range (IQR); whiskers, range; bars, standard deviation. (e) Transmission
6 electron micrograph of uninfected cholangiocyte organoids (left panel) and cholangiocyte
7 organoids infected with SARS-CoV-2 in the absence (central panel) or presence of CDCA
8 (right panel) showing key morphological features of viral infection and cell death, such as
9 production of viral particles, formation of pathologic vacuoles (Vc) and swollen mitochondria
10 (Mt). N=3 independent experiments. Scale bars 5 μ m.

11

12 **Extended Data Fig. 3. FXR is present and active in tissues affected by COVID-19 and**
13 **their corresponding CDCA-treated organoids. (a-b)** Immunofluorescence images
14 confirming expression of FXR in primary human gallbladder, lungs and intestinal tissue (a)
15 and in corresponding primary organoids treated with physiological levels of bile acids (CDCA,
16 10 μ M) (b). N=4 independent experiments. White scale bars 100 μ m; grey scale bar 25 μ m.
17 (c) QPCR analysis validating expression of FXR and its downstream effector SHP in primary
18 tissue and corresponding organoids in presence or absence of physiological levels of bile
19 acids (CDCA). CDCA treatment increases FXR and SHP expression in organoids to levels
20 that are closer to primary tissue. Housekeeping gene, HMBS; n=4 independent experiments;
21 one-way ANOVA adjusted for multiple comparisons; centre line, median; box, interquartile
22 range (IQR); whiskers, range; bars, standard deviation. GCOs, gallbladder cholangiocyte
23 organoids; AOs, airway organoids; IOs, intestinal organoids.

24

25 **Extended Data Fig. 4. UDCA and ZGG require FXR to reduce ACE2 and SARS-CoV-2**

1 **infection. (a-b)** Immunofluorescence **(a)** and QPCR **(b)** showing downregulation of FXR
2 expression following FXR knock-down (KD) in cholangiocyte organoids. Scale bars 25 μ m.
3 Housekeeping gene HMBS. One-way ANOVA adjusted for multiple comparisons; n=4
4 independent experiments; centre line, median; box, interquartile range; whiskers, range;
5 bars, standard deviation. **(c)** QPCR on FXR KD cholangiocyte organoids showing no change
6 in the expression of ACE2 and the FXR downstream effector SHP following treatment with
7 CDCA, UDCA or ZGG, demonstrating that FXR is indispensable for regulating ACE2 and
8 SHP through these compounds. ACE2 and SHP expression in wild-type organoids shown in
9 Fig. 1c and ED Fig. 5a. Housekeeping gene, HMBS; n=4; one-way ANOVA adjusted for
10 multiple comparisons; ns, non-significant; centre line, median; box, interquartile range;
11 whiskers, range; bars, standard deviation. **(d)** QPCR quantifying SARS-CoV-2 RNA 24 hours
12 post infection in FXR KD cholangiocyte organoids treated with CDCA, UDCA or ZGG. SARS-
13 CoV-2 infection in the presence of FXR is shown in Fig. 1e. Housekeeping gene, GAPDH;
14 n=4 independent experiments; one-way ANOVA adjusted for multiple comparisons; centre
15 line, median; box, interquartile range; whiskers, range; bars, standard deviation. (CDCA,
16 UDCA and ZGG concentration, 10 μ M). **(e)** Schematic illustrating the luciferase reporter
17 construct containing the FXR responsive element IR-1 identified in Fig. 1a and the
18 mutagenesis strategy employed in panel (f). **(f)** Luciferase reporter assay in HEK293 cells
19 showing the transcriptional activity associated with the IR-1 located in the ACE2 promoter
20 upon treatment with CDCA, UDCA or ZGG. Site-directed mutagenesis on IR-1 abolishes FXR
21 binding/transactivation confirming the specificity of FXR binding on the ACE2 IR-1. IR-1
22 located in the SHP promoter used as positive control. N=3 independent experiments; one-
23 way ANOVA adjusted for multiple comparisons; bars, standard deviations. (CDCA, UDCA
24 and ZGG concentration, 50 μ M).

25

1 **Extended Data Fig. 5. FXR modulation in biliary, airway and intestinal.** (a) QPCR
2 analysis in primary airway, biliary and intestinal organoids demonstrating that CDCA
3 activates FXR, while UDCA and ZGG inhibit it, as evidenced by corresponding changes in
4 the expression of the FXR downstream target SHP. Housekeeping gene, HMBS; n=4
5 independent experiments; one-way ANOVA adjusted for multiple comparisons; centre line,
6 median; box, interquartile range (IQR); whiskers, range; bars, standard deviation. (b)
7 Immunofluorescence showing ACE2 expression levels in primary organoids in absence of
8 bile acids. The panel is complementary to Fig. 1d showing the modulation of ACE2 following
9 FXR activation (CDCA) and inhibition (UDCA/ZGG). N=4 independent experiments. Yellow
10 scale bars 50 μm ; grey scale bar 25 μm . (c) Flow cytometry histograms showing changes in
11 ACE2 levels upon modulation of FXR activity in primary airway, biliary and intestinal
12 organoids. n=3 independent experiments. (CDCA, UDCA and ZGG concentration, 10 μM).
13 (d) Dose-response curves showing the effect of 0.01 μM – 1 mM of CDCA, UDCA and ZGG
14 on the expression of ACE2 in primary airway, biliary and intestinal organoids (n=3
15 independent experiments). Response defined as percentage of the maximal ACE2
16 expression level for each condition via QPCR. Bars, SEM. (e) Percentage of non-viable cells
17 following treatment of airway, biliary and intestinal organoids with CDCA, UDCA and ZGG at
18 a range of 0.1 μM – 100 μM showing that these compounds cause minimal cell death within
19 the tested range. N=3 independent experiments. Bars, range. (f) Resazurin assay
20 (PrestoBlue) showing that treatment with 10 μM of CDCA, UDCA or ZGG does not affect
21 cellular viability. N=4 independent experiments; one-way ANOVA adjusted for multiple
22 comparisons; ns, non-significant; centre line, median; box, interquartile range (IQR);
23 whiskers, range; bars, standard deviation.

24
25 **Extended Data Fig. 6. ACE2 downregulation is required for the UDCA/ZGG-mediated**

1 **reduction in SARS-CoV-2 infection. (a-b)** QPCR analysis **(a)** and immunofluorescence **(b)**
2 illustrating ACE2 and FXR expression in wild-type HEK293 cells and HEK293T cells stably
3 expressing ACE2. Primary human airway tissue used as positive control. Housekeeping
4 gene, HMBS; n=4; one-way ANOVA adjusted for multiple comparisons; centre line, median;
5 box, interquartile range (IQR); whiskers, range; bars, standard deviation. Scale bars 100 μ m.
6 **(c)** SARS-CoV-2 infection of HEK293T cells genetically engineered to stably express ACE2.
7 Cells were treated with the indicated doses of CDCA, UDCA or ZGG, infected with SARS-
8 CoV-2 at an MOI of 0.01, and analysed after 24 h. The SARS-CoV-2 RdRp inhibitor
9 remdesivir and a neutralising antibody cocktail blocking the interaction between SARS-CoV-
10 2 spike and ACE2 (REGN-COV2) were included as positive controls. N=3; one-way ANOVA
11 adjusted for multiple comparisons; mean values \pm SEM;

12
13 **Extended Data Figure 7. FXR inhibition reduces ACE2 levels *in vivo*.** **(a)** Schematic
14 representation of the experiment performed. **(b)** QPCR showing that treatment with UDCA in
15 FVB/N mice reduces ACE2 levels in lung, gallbladder and intestinal tissue. Housekeeping
16 gene, GAPDH; n=4 animals per group (UDCA vs. no UDCA control group, see methods);
17 unpaired two-tailed t-test; centre line, median; box, interquartile range (IQR); whiskers, range;
18 bars, standard deviation. **(c)** Immunofluorescence images showing ACE2 levels upon
19 treatment with UDCA in respiratory, biliary and intestinal epithelium in FVB/N mice. N=4 mice
20 per group. White scale bars 100 μ m; yellow scale bars 50 μ m. **(d)** QPCR showing that
21 treatment with UDCA in Syrian golden hamsters reduces ACE2 levels in the gallbladder and
22 intestinal tissue. Housekeeping gene, GAPDH; n=5 vehicle/No UDCA group vs n=3 UDCA
23 group; unpaired two-tailed t-test; centre line, median; box, interquartile range (IQR); whiskers,
24 range; bars, standard deviation. **(e)** Immunofluorescence images showing ACE2 levels upon
25 treatment with UDCA in biliary and intestinal epithelium in Syrian golden hamsters. N=3

1 hamsters per group. White scale bars 100 μm .

2

3 **Extended Data Figure 8. UDCA plasma concentration *in vivo*.** (a) UDCA concentration in
4 the plasma of hamsters over 7 days of treatment with 416 mg/kg/day of UDCA. N=6
5 animals/group; line, median. (b) Viral titre showing levels of infectious virus as measured by
6 plaque assay in lungs in directly inoculated hamsters and sentinel animals treated with UDCA
7 or vehicle and co-housed with infected animals. Samples were collected after 4 days of co-
8 housing. N=6 UDCA vs n=3 vehicle animals; Kruskal-Wallis test with Dunn's correction for
9 multiple comparisons. Animals from each experiment are represented with different symbols;
10 line, median.

11

12 **Extended Data Figure. 9. FXR inhibition reduces SARS-CoV-2 infection in human**
13 **organs *ex vivo*.** (a) Photograph and schematic of the liver *ex situ* normothermic perfusion
14 (ESNP) experiment performed; including type of samples harvested and timeline. 0h: 0 hours
15 baseline sample collection and UDCA/carrier administration. The 0h samples were collected
16 immediately prior to UDCA administration. 12h: 12 hours after UDCA/carrier administration.
17 For each timepoint, 4 independent tissue samples were obtained from the grafts' gallbladder
18 and used for ACE2 measurement and viral infection (n=4 gallbladder tissue samples per
19 timepoint). (b) ACE2 enzymatic activity measurement showing that ESNP with UDCA
20 reduces ACE2 activity in the circulating perfusate, compared to carrier only control. N=4
21 independent samples; unpaired two-tailed t-test; centre line, median; box, interquartile range
22 (IQR); whiskers, range; bars, standard deviation. (c) Immunofluorescence images showing
23 ACE2 expression in gallbladder cholangiocytes and cells of the vasculature (smooth muscle
24 and endothelial cells) in human livers before and after ESNP with UDCA/carrier. N=4
25 independent samples. White scale bars 100 μm ; yellow scale bars 50 μm , grey scale bars 25

1 μm . (d) QPCR demonstrating that ESNP with UDCA reduces ACE2 levels in gallbladder
2 cholangiocytes, compared to carrier only control. Housekeeping gene, HMBS; n=4; unpaired
3 two-tailed t-test; centre line, median; box, interquartile range (IQR); whiskers, range; bars,
4 standard deviation. (e-f) QPCR (e) and immunofluorescence (f) showing that UDCA reduces
5 SARS-CoV-2 infection in human gallbladder *ex vivo*. Housekeeping gene, GAPDH; n=4; one-
6 way ANOVA adjusted for multiple comparisons; centre line, median; box, interquartile range
7 (IQR); whiskers, range; bars, standard deviation. Scale bars 25 μm . (UDCA, concentration,
8 2000 ng/ml).

9
10 **Extended Data Fig. 10. UDCA is associated with lower ACE2 levels in patients with**
11 **PBC.** (a) Schematic illustrating the patient cohorts compared in (b). (b) Multiple linear
12 regression analysis of serum ACE2 demonstrates that UDCA correlates with lower ACE2
13 levels in patients with primary biliary cholangitis (PBC) receiving UDCA (n=308) vs. PBC
14 patients naïve to treatment (n=62). Values plotted are β coefficients. (BMI, body mass index;
15 ALP, alkaline phosphatase). Bars, 95% confidence interval.

18 **Additional references**

- 19 50. Tysoe, O. C. *et al.* Isolation and propagation of primary human cholangiocyte
20 organoids for the generation of bioengineered biliary tissue. *Nat. Protoc.* **14**, (2019).
- 21 51. Bjerknes, M. & Cheng, H. Methods for the isolation of intact epithelium from the
22 mouse intestine. *Anat. Rec.* **199**, 565–574 (1981).
- 23 52. Papa, G. *et al.* Furin cleavage of SARS-CoV-2 Spike promotes but is not essential for
24 infection and cell-cell fusion. *PLoS Pathog.* **17**, (2021).
- 25 53. Balasubramaniyan, N., Luo, Y., Sun, A. Q. & Suchy, F. J. SUMOylation of the

- 1 farnesoid X receptor (FXR) regulates the expression of FXR target genes. *J. Biol.*
2 *Chem.* **288**, 13850–13862 (2013).
- 3 54. Termini, E. *et al.* Methods of inactivation of SARS-CoV-2 for downstream biological
4 assays. **21**, 1–9 (2020).
- 5 55. Cantuti-Castelvetri, L. *et al.* Neuropilin-1 facilitates SARS-CoV-2 cell entry and
6 infectivity. *Science (80-.)*. **370**, 1–9 (2020).
- 7 56. Sridhar, S. *et al.* A blueprint for the implementation of a validated approach for the
8 detection of SARS-Cov2 in clinical samples in academic facilities. *Wellcome Open*
9 *Res.* **5**, 110 (2020).
- 10 57. Gerber, P. P. *et al.* A protease-activatable luminescent biosensor and reporter cell
11 line for authentic SARS-CoV-2 infection. *bioRxiv* 2021.03.22.435957 (2021).
- 12 58. Fickert, P. *et al.* Effects of ursodeoxycholic and cholic acid feeding on hepatocellular
13 transporter expression in mouse liver. *Gastroenterology* **121**, 170–183 (2001).
- 14 59. Morrison, M. I. *et al.* Use of Phosphodiesterase Inhibition During Ex-Vivo Lung
15 Perfusion of Donor Lungs Unsuitable for Transplantation. *J. Hear. Lung Transplant.*
16 **38**, S321 (2019).
- 17 60. Sachs, N. *et al.* Long-term expanding human airway organoids for disease modeling.
18 *EMBO J.* **38**, 1–20 (2019).
- 19 61. Marjot, T. *et al.* SARS-CoV-2 infection in patients with autoimmune hepatitis. *J.*
20 *Hepatol.* 1–9 (2021) doi:10.1016/j.jhep.2021.01.021.

Figure 1. FXR modulates ACE2 expression and SARS-CoV-2 infection

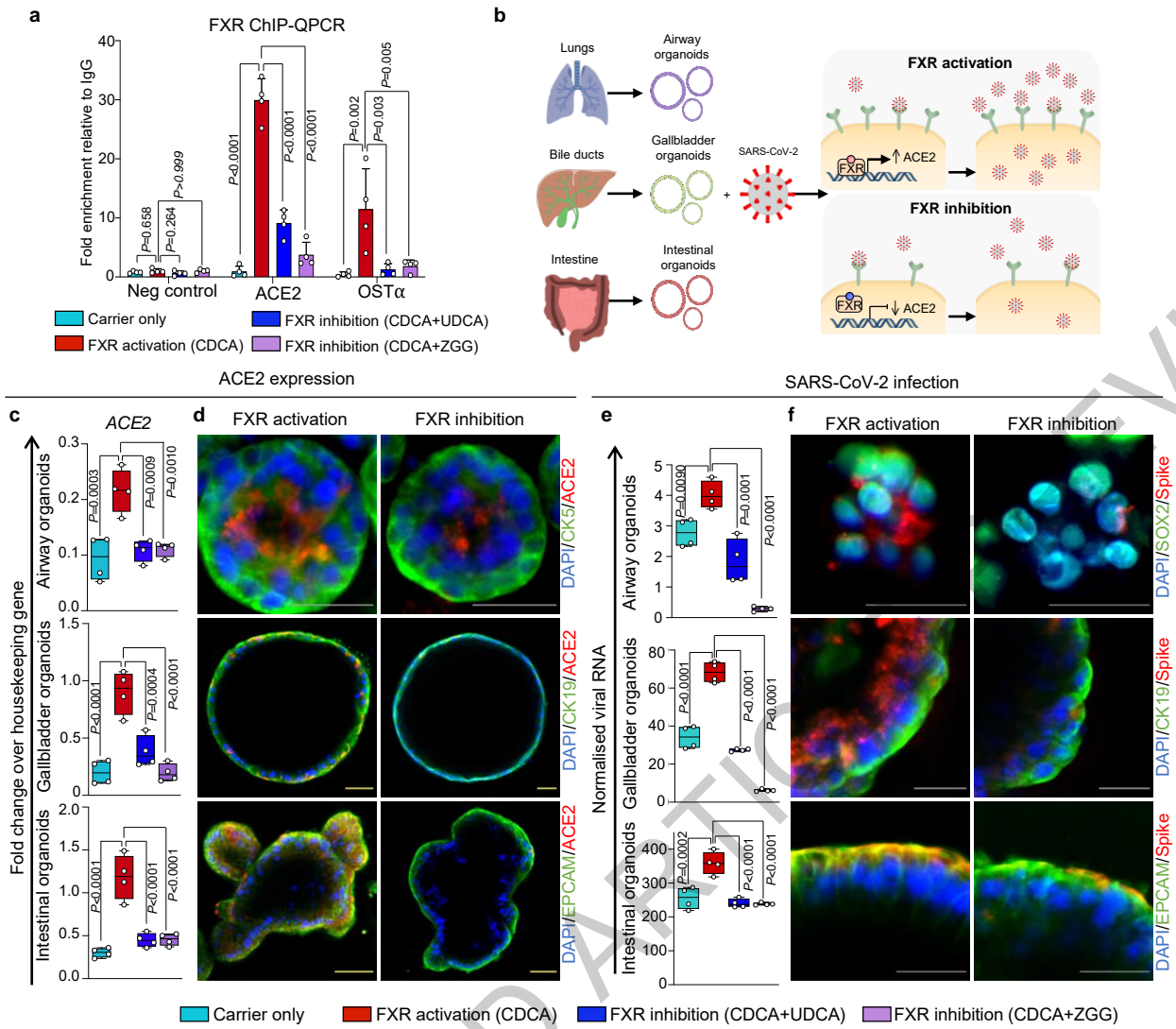


Figure 2. FXR inhibition reduces ACE2 and SARS-CoV-2 infection *in vivo*.

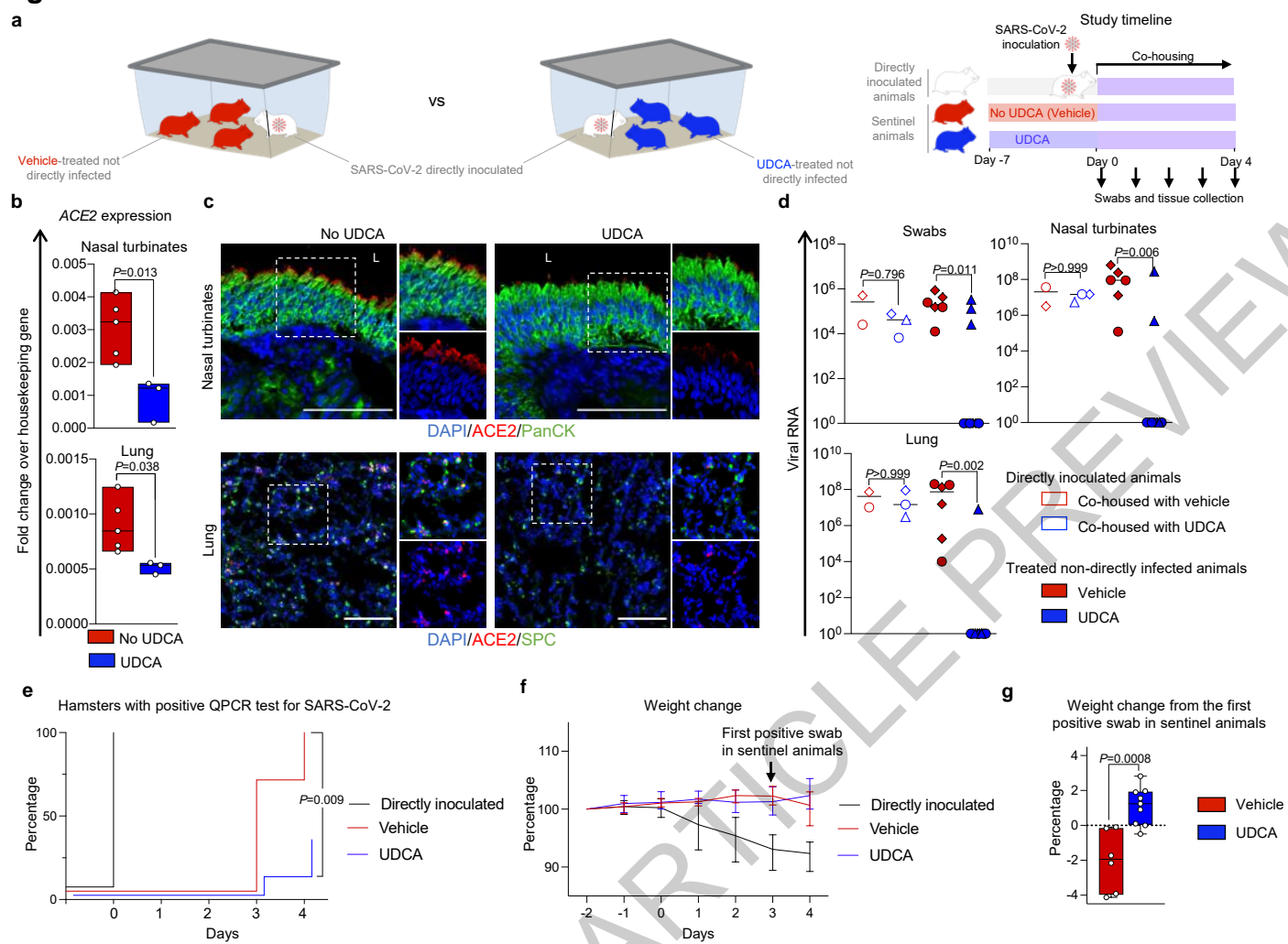
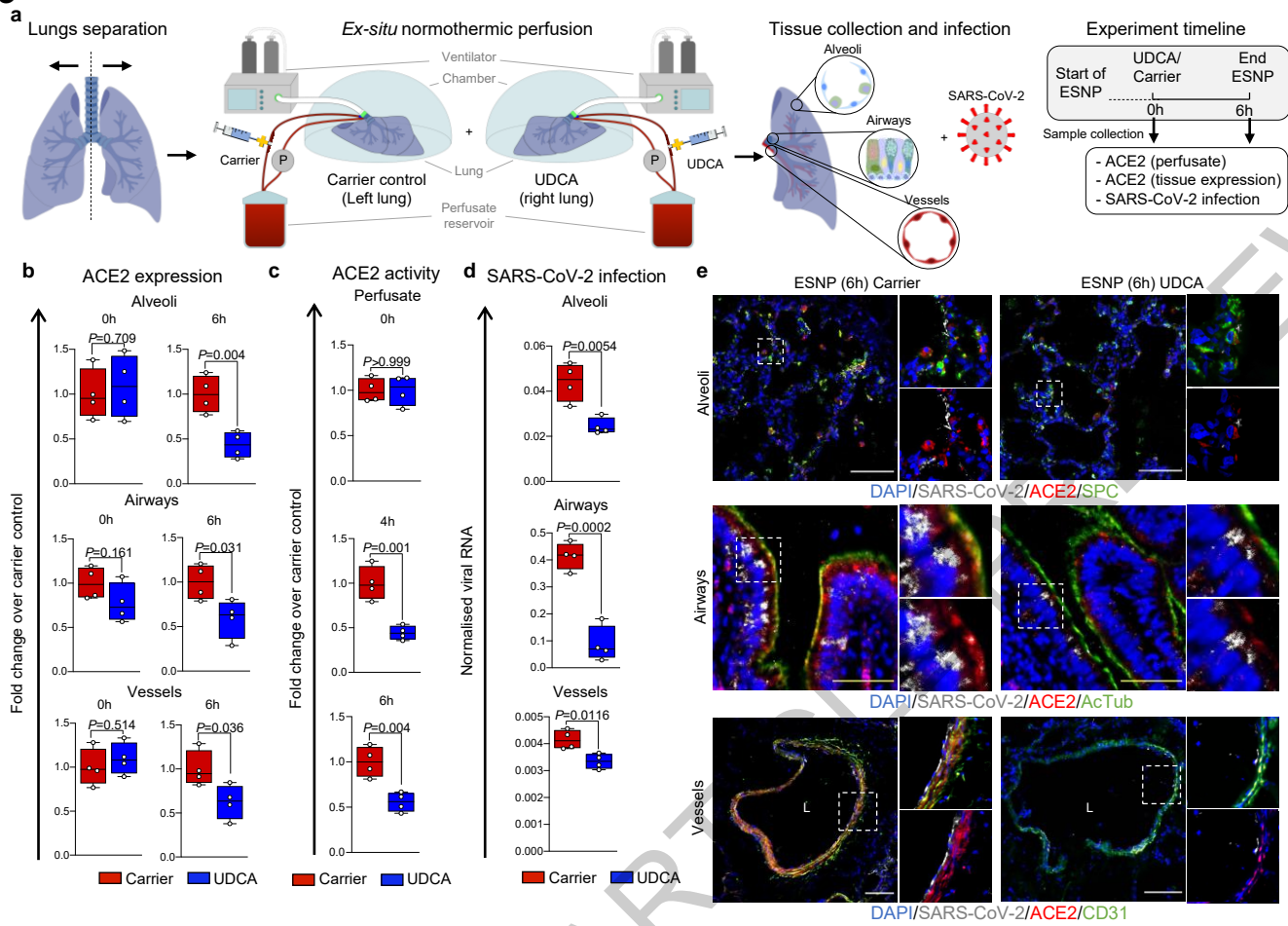
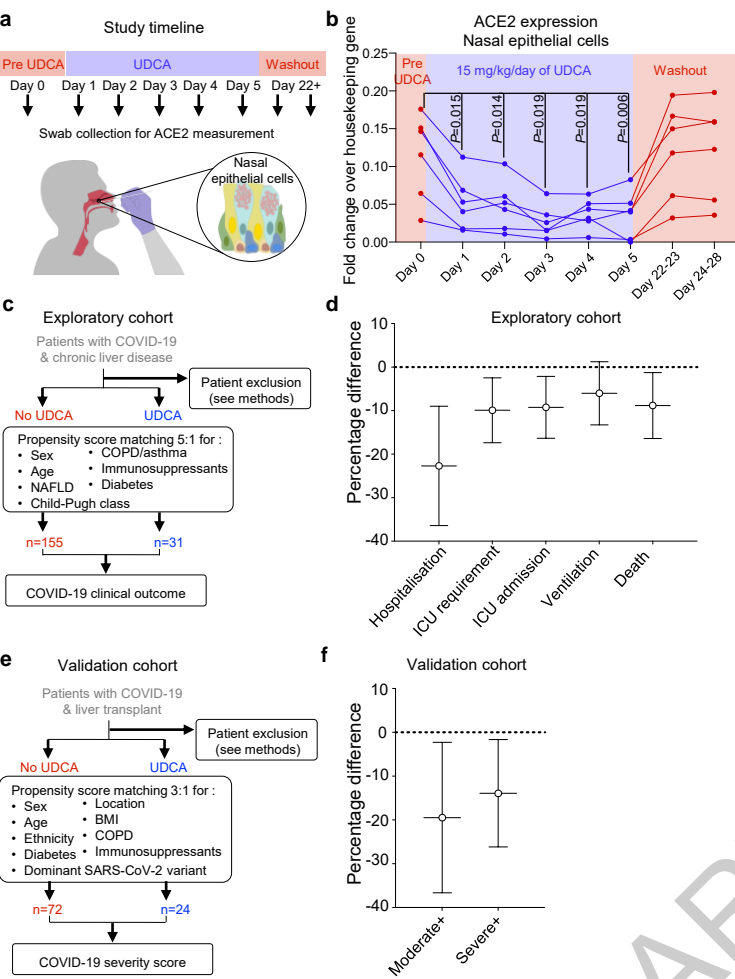


Figure 3. FXR inhibition reduces ACE2 levels and SARS-CoV-2 infection in a human lung *ex vivo*



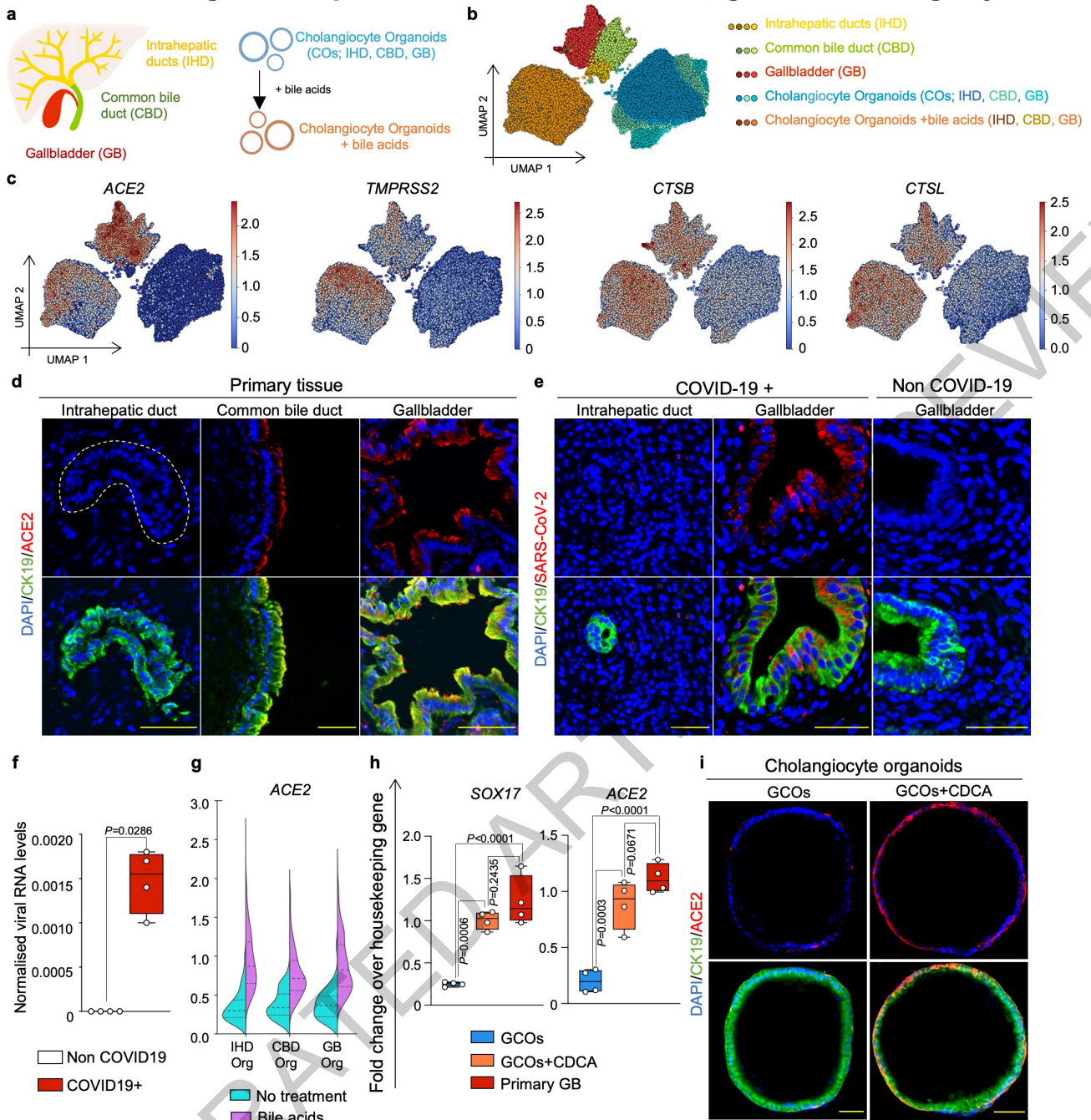
ACCELERATED ARTICLE

Figure 4. UDCA is associated with lower ACE2 levels and better clinical outcome in COVID-19 patients

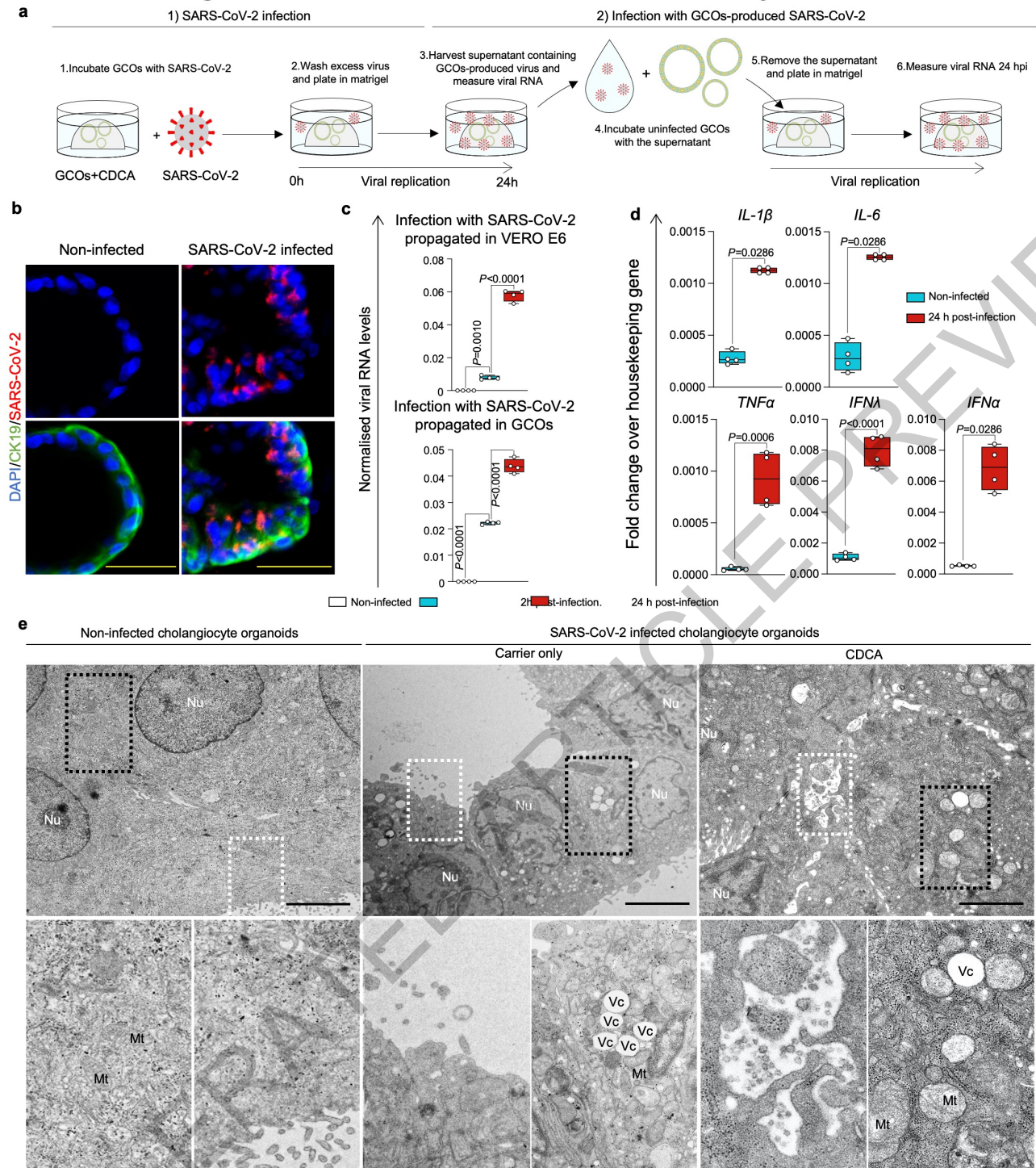


ACCELERATED ARTICLE PREVIEW

Extended Data Figure 1. Expression of SARS-CoV-2 entry genes in cholangiocytes

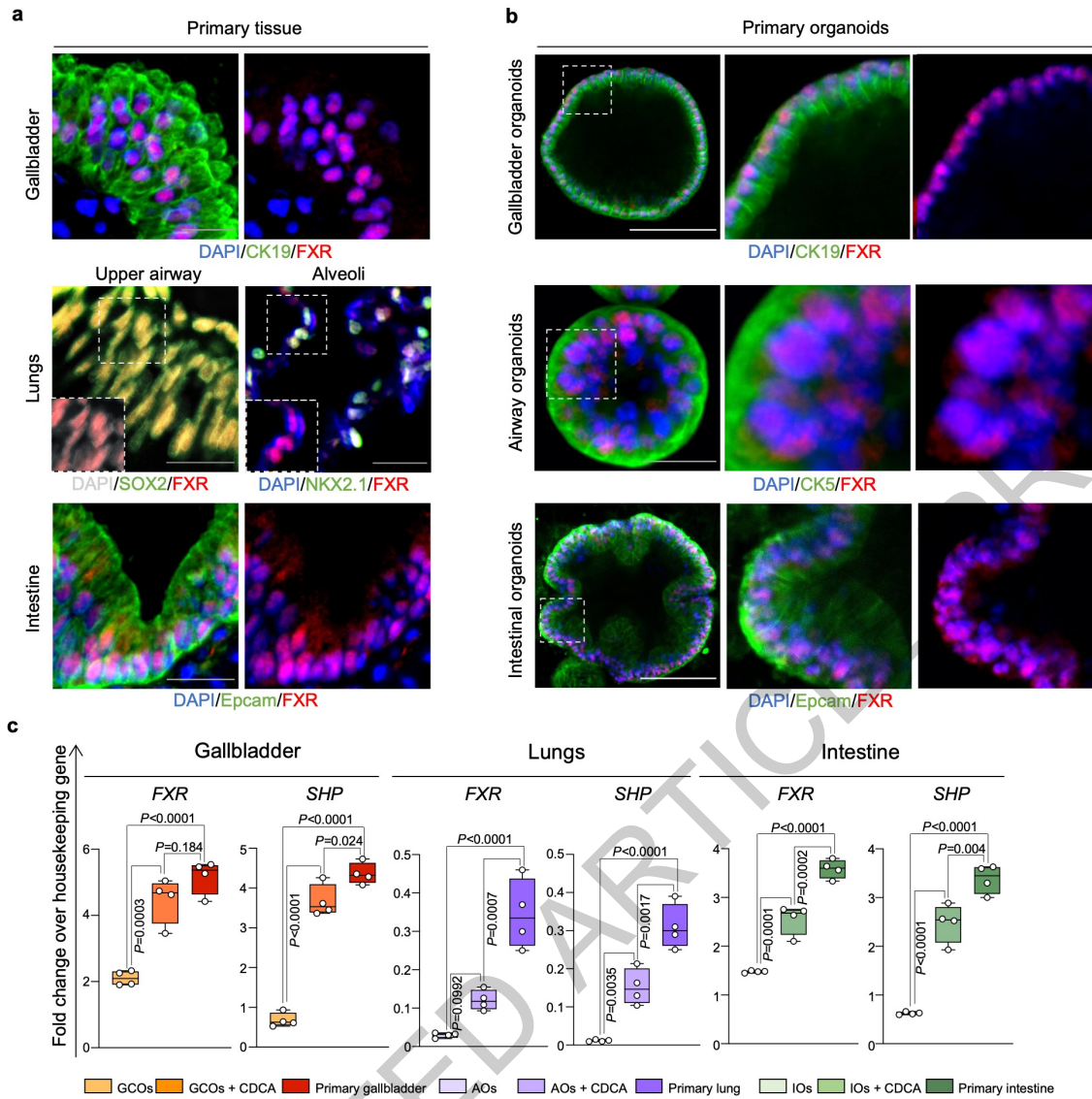


Extended Data Figure 2. CDCA-treated GCOs can be infected by SARS-CoV-2

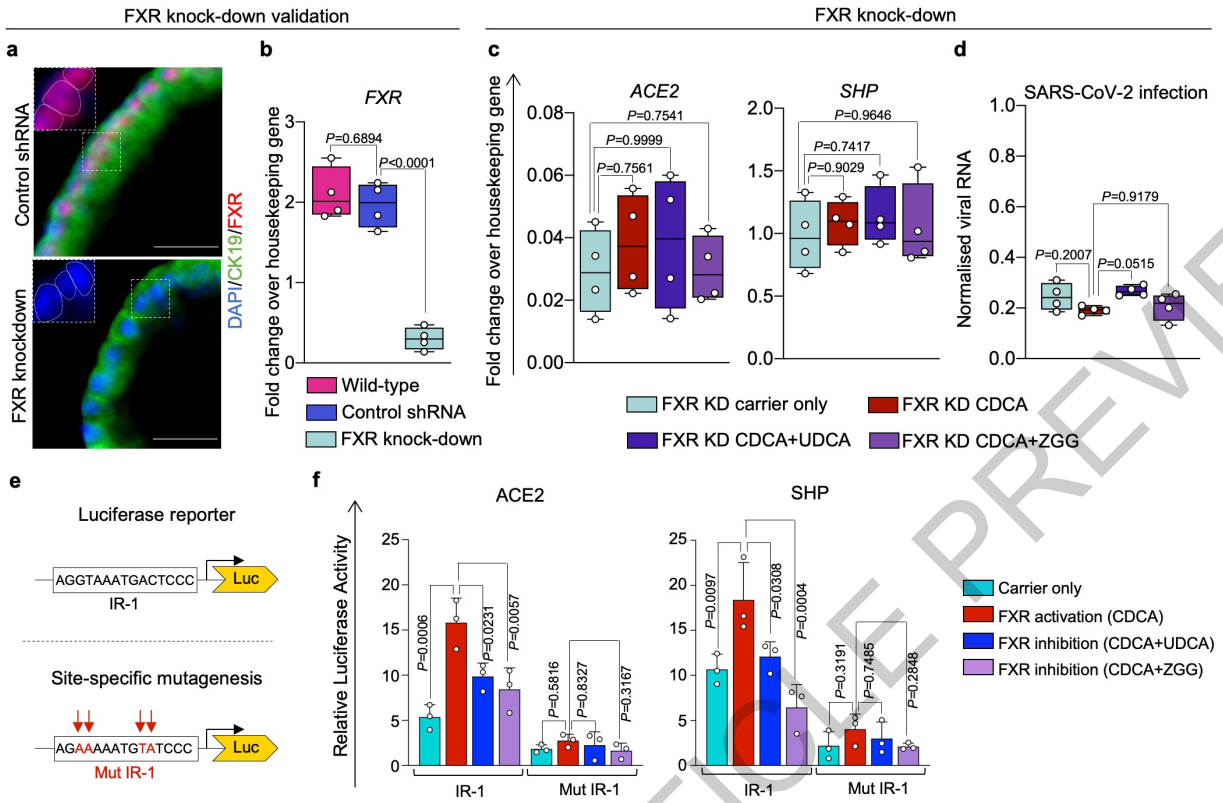


ACCEPTED MANUSCRIPT

Extended Data Figure 3. FXR is present and active in tissues affected by COVID-19 and their corresponding CDCA-treated organoids

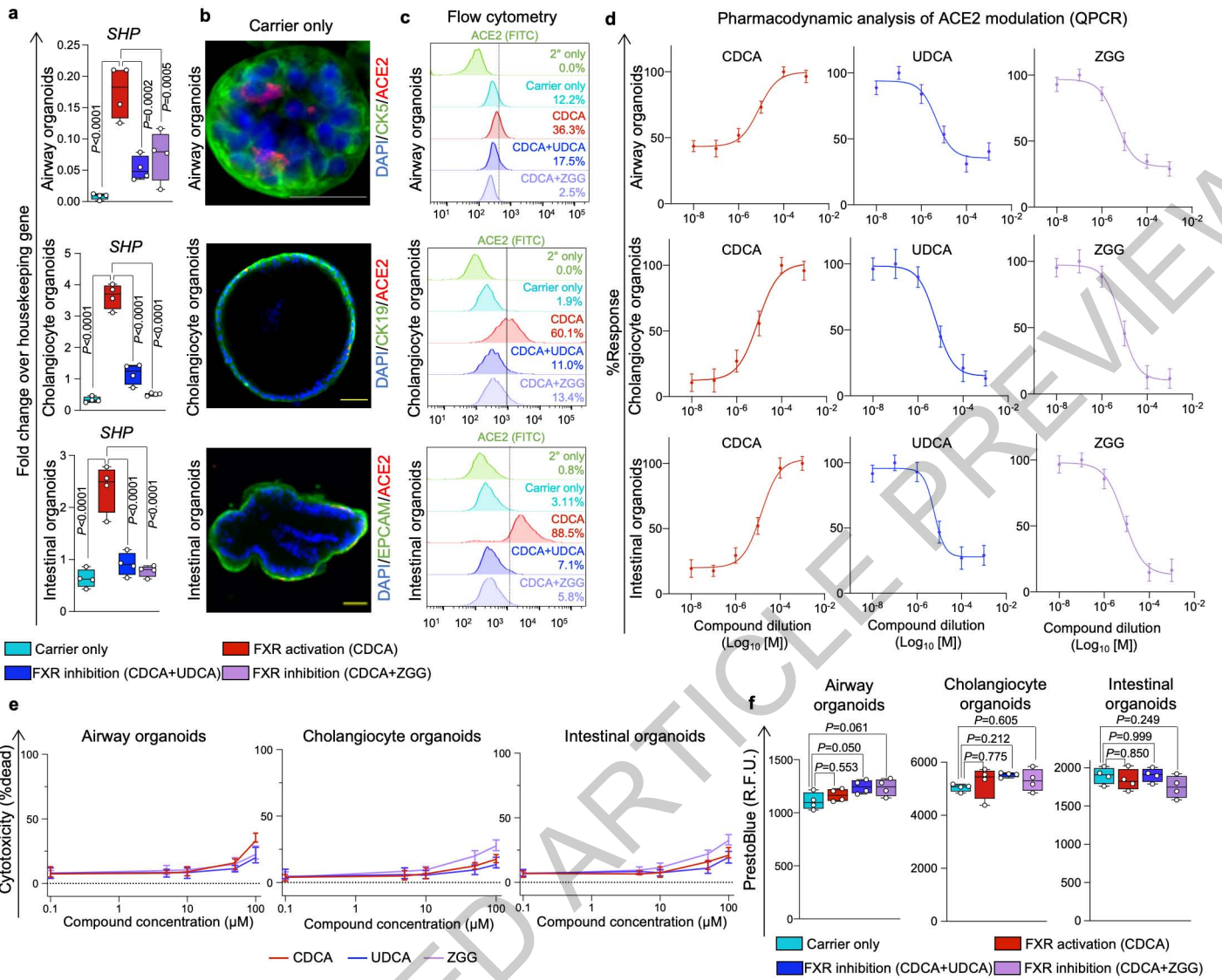


Extended Data Figure 4. FXR is indispensable for prevention of SARS-CoV-2 infection via UDCA and ZGG

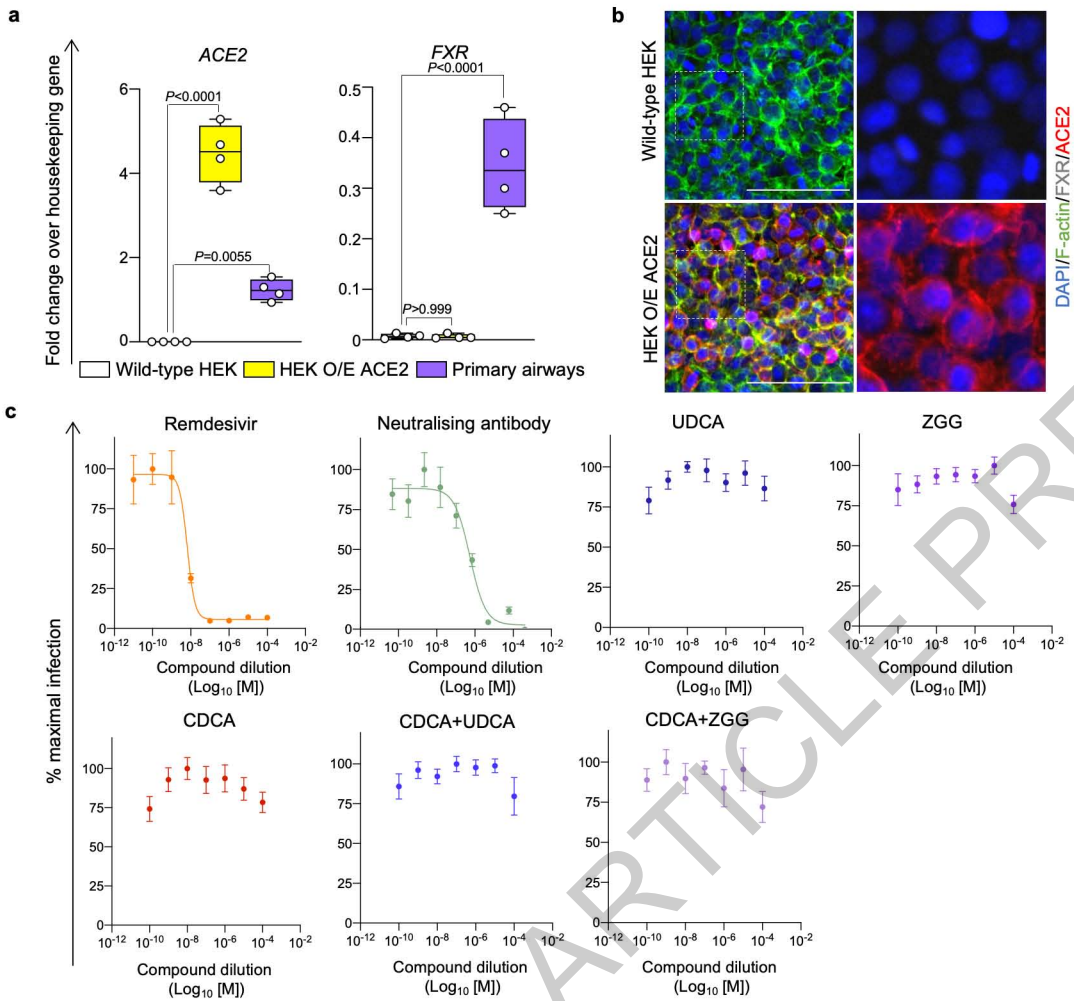


ACCELERATED ARTICLE PREVIEW

Extended Data Fig 5. Effects of FXR modulation in biliary, airway and intestinal organoids

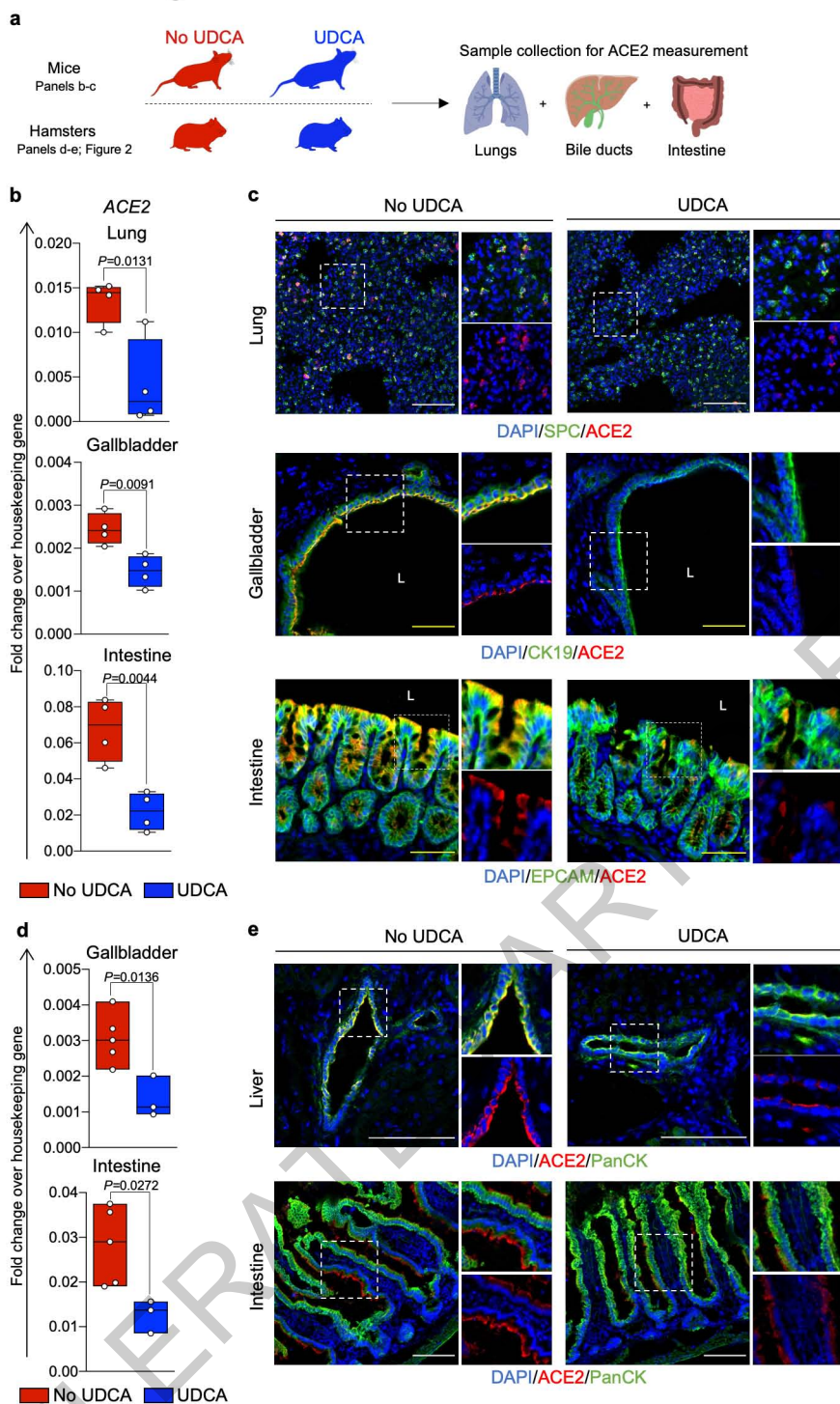


Extended Data Figure 6. ACE2 downregulation is required for the UDCA/ZGG-mediated reduction in SARS-CoV-2 infection



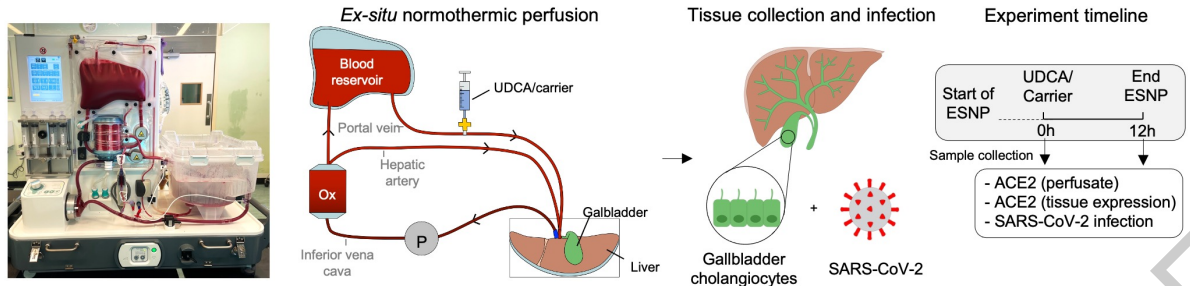
ACCELERATED ARTICLE PREVIEW

Extended Data Figure 7. FXR inhibition reduces ACE2 *in vivo*

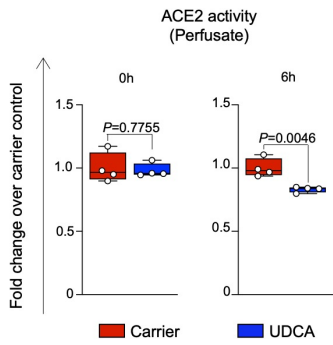


Extended Data Figure 9. FXR inhibition reduces SARS-CoV-2 infection in a human liver ex vivo

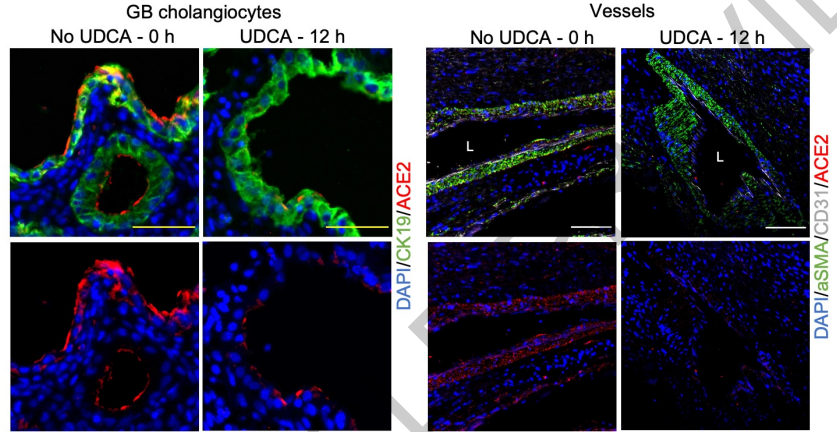
a



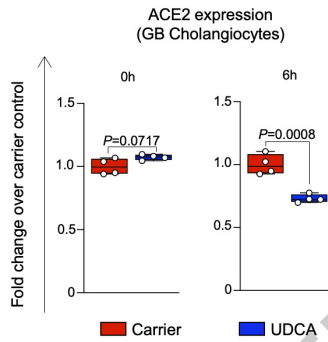
b



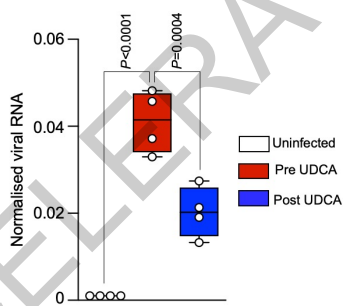
c



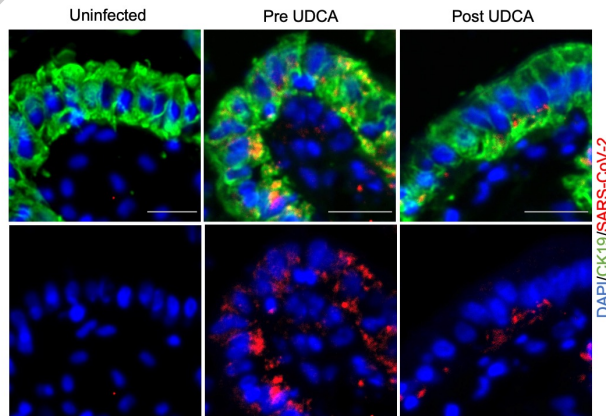
d



e

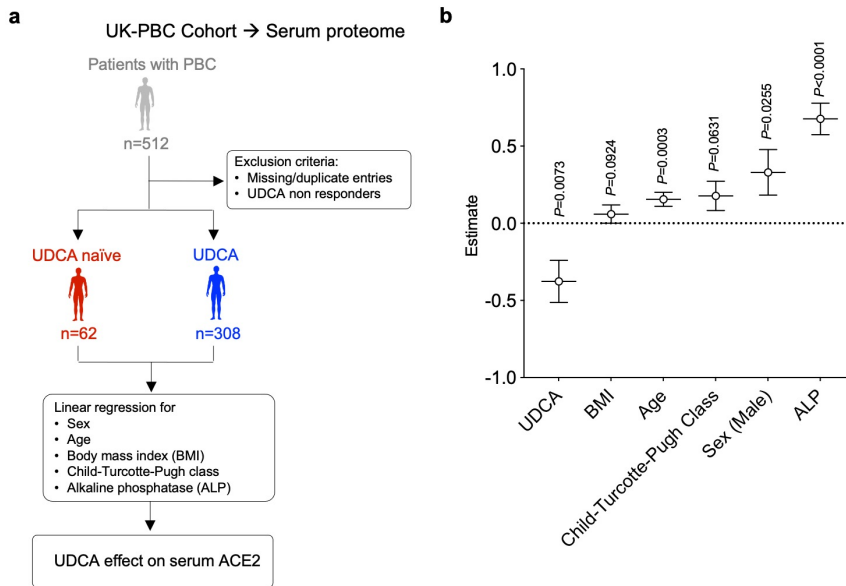


f



ACCELERATE

Extended Data Figure 10. UDCA is associated with lower ACE2 levels in patients with PBC



ACCELERATED ARTICLE PREVIEW

Reporting Summary

Nature Research wishes to improve the reproducibility of the work that we publish. This form provides structure for consistency and transparency in reporting. For further information on Nature Research policies, see our [Editorial Policies](#) and the [Editorial Policy Checklist](#).

Statistics

For all statistical analyses, confirm that the following items are present in the figure legend, table legend, main text, or Methods section.

n/a Confirmed

- The exact sample size (n) for each experimental group/condition, given as a discrete number and unit of measurement
- A statement on whether measurements were taken from distinct samples or whether the same sample was measured repeatedly
- The statistical test(s) used AND whether they are one- or two-sided
Only common tests should be described solely by name; describe more complex techniques in the Methods section.
- A description of all covariates tested
- A description of any assumptions or corrections, such as tests of normality and adjustment for multiple comparisons
- A full description of the statistical parameters including central tendency (e.g. means) or other basic estimates (e.g. regression coefficient) AND variation (e.g. standard deviation) or associated estimates of uncertainty (e.g. confidence intervals)
- For null hypothesis testing, the test statistic (e.g. F , t , r) with confidence intervals, effect sizes, degrees of freedom and P value noted
Give P values as exact values whenever suitable.
- For Bayesian analysis, information on the choice of priors and Markov chain Monte Carlo settings
- For hierarchical and complex designs, identification of the appropriate level for tests and full reporting of outcomes
- Estimates of effect sizes (e.g. Cohen's d , Pearson's r), indicating how they were calculated

Our web collection on [statistics for biologists](#) contains articles on many of the points above.

Software and code

Policy information about [availability of computer code](#)

Data collection BD FACS Diva 8.0.3 (BD Bioscience; for analyses on LSR-II); ZEN 2011 SP7 (Zeiss) on a Zeiss LSM 700 or 710 confocal microscope; QuantStudio 5 384 Well Block (Thermo Fisher); SoftMax Pro 5.4.4 on SpectraMax M2 (Molecular Devices); HT7800 TEM operating software version 01.21 (Hitachi) on a HT7800 transmission electron microscope (Hitachi High Technologies, Japan).

Data analysis Microsoft Excel v 16.19; GraphPad Prism 9; Stata 15.1 (StataCorp, College Station, TX, USA); FlowJo v 10; ImageJ 2.0.0-rc-69/1.53f; Anaconda-Navigator 1.9.12; Jupyter Notebook 6.0.3; Rstudio (version 1.1.463).

For manuscripts utilizing custom algorithms or software that are central to the research but not yet described in published literature, software must be made available to editors and reviewers. We strongly encourage code deposition in a community repository (e.g. GitHub). See the Nature Research [guidelines for submitting code & software](#) for further information.

Data

Policy information about [availability of data](#)

All manuscripts must include a [data availability statement](#). This statement should provide the following information, where applicable:

- Accession codes, unique identifiers, or web links for publicly available datasets
- A list of figures that have associated raw data
- A description of any restrictions on data availability

Single-cell RNA sequencing data are available on ArrayExpress. Accession number: E-MTAB-8495. Source data are provided with this paper.

Field-specific reporting

Please select the one below that is the best fit for your research. If you are not sure, read the appropriate sections before making your selection.

Life sciences Behavioural & social sciences Ecological, evolutionary & environmental sciences

For a reference copy of the document with all sections, see [nature.com/documents/nr-reporting-summary-flat.pdf](https://www.nature.com/documents/nr-reporting-summary-flat.pdf)

Life sciences study design

All studies must disclose on these points even when the disclosure is negative.

Sample size

No statistical analyses were performed to predetermine sample size. The samples size for each experiment is specified in the corresponding figure legend. At least 4 biological replicates were used for in vitro experiments. At least 4 mice and 3 hamsters per group were used for in vivo experiments. For ESNP experiments 4 independent samples from the same organ before and after UDCA treatment were used for each tissue. For animal experiments, group sizes were estimated based on previous study variance and cage capacity. For in vitro and ex vivo experiments, sample size of n=4 was chosen as the minimum number of samples required to adequately provide standard deviation, median and range. For human prospective study, the maximum number of individuals that could be recruited during the study period was used. For retrospective clinical studies, the maximum number of individuals in our cohort meeting the study criteria was used.

Data exclusions

In the COVID-Hep.net and SECURE-Liver registries data were filtered to remove duplicate entries, those with incomplete records, those with prior liver transplantation, those younger than 18 years of age and older than 90 years of age, and those without laboratory confirmed infection. Due to the absence of patients with Alcohol Related Liver Disease (ARLD) in the UDCA group, patients with ARLD were excluded from the analysis in both groups. In the UK-PBC proteomic study data were filtered to remove duplicate entries, those with incomplete records and those classified as non-responders to treatment according to PARIS2 criteria. For the study involving participants from the University Medical Centre Hamburg-Eppendorf, two individuals were excluded because of undetectable RNA levels in nasopharyngeal swabs. No further data were excluded from the analyses presented in this manuscript. In the VOCAL cohort of liver transplant recipients, participants who had no COVID-19 infection, were unvaccinated or developed COVID-19 within 30 days from their first UDCA prescription were excluded.

Replication

All experiments were repeated and validated as stated in the respective figure legends.

Randomization

No formal randomization method was used to assign primary organoids to study groups. For in vitro experiments primary organoids were plated in 24-well plates and different wells of the same plates were randomly allocated to one of the 4 experimental groups (Carrier only; CDCA; CDCA+UDCA; CDCA+ZGG). For in vivo experiments, animals were randomly allocated to the treatment or control group. For analysis of the UK-PBC proteomic cohort covariables such as age, sex, BMI, stage of liver disease (Child-Turcotte-Pugh class) and ALP were controlled for via multiple linear regression. For analysis of the COVID-Hep.net and SECURE-Liver registries patient cohort covariables such as age, sex, diabetes, NAFLD and stage of liver disease (Child-Turcotte-Pugh class) were controlled for via propensity score matching analyses. For the VOCAL cohort of liver transplant recipients covariable such as age, sex, ethnicity, location within the United States, diabetes, BMI, COPD, type of immunosuppressive therapy (calcineurin inhibitor with or without anti-metabolite therapy) and dominant SARS-CoV-2 variant were controlled for via propensity score matching analyses.

Blinding

Blinding was performed for all experiments. If blinding was not possible at the time of the experiment, specifically in directly inoculated hamster samples and organs perfused ex situ, samples were collected and anonymised and sample processing was subsequently performed by a blinded researcher.

Reporting for specific materials, systems and methods

We require information from authors about some types of materials, experimental systems and methods used in many studies. Here, indicate whether each material, system or method listed is relevant to your study. If you are not sure if a list item applies to your research, read the appropriate section before selecting a response.

Materials & experimental systems

n/a	Involvement in the study
<input type="checkbox"/>	<input checked="" type="checkbox"/> Antibodies
<input type="checkbox"/>	<input checked="" type="checkbox"/> Eukaryotic cell lines
<input checked="" type="checkbox"/>	<input type="checkbox"/> Palaeontology and archaeology
<input type="checkbox"/>	<input checked="" type="checkbox"/> Animals and other organisms
<input type="checkbox"/>	<input checked="" type="checkbox"/> Human research participants
<input checked="" type="checkbox"/>	<input type="checkbox"/> Clinical data
<input checked="" type="checkbox"/>	<input type="checkbox"/> Dual use research of concern

Methods

n/a	Involvement in the study
<input checked="" type="checkbox"/>	<input type="checkbox"/> ChIP-seq
<input type="checkbox"/>	<input checked="" type="checkbox"/> Flow cytometry
<input checked="" type="checkbox"/>	<input type="checkbox"/> MRI-based neuroimaging

Antibodies

Antibodies used

A full list of the antibodies used can be found in Supplementary Table S1.

Validation

Anti-ACE2; R&D; AF933; dilution 1:50 / 1:100; https://resources.rndsystems.com/pdfs/datasheets/af933.pdf?v=20221029&_ga=2.68548246.663064109.1667061858-1717995244.1667061858.

Anti-ACE2; abcam; ab15348; dilution 1:500; <https://www.abcam.com/ace2-antibody-ab15348.html>.

Anti-ACE2; abcam; ab108209; dilution 1:500 / 1:100; <https://www.abcam.com/ace2-antibody-epr4436-ab108209.html>.

Anti-EPCAM; R&D; MAB9601; dilution 1:50 / 1:100; https://resources.rndsystems.com/pdfs/datasheets/mab9601.pdf?v=20221029&_ga=2.232101272.663064109.1667061858-1717995244.1667061858.

Anti-EPCAM; R&D; AF960; dilution 1:100; https://resources.rndsystems.com/pdfs/datasheets/af960.pdf?v=20221029&_ga=2.232101272.663064109.1667061858-1717995244.1667061858.

Anti-Cytokeratin 19; abcam; ab7754; dilution 1:100; <https://www.abcam.com/cytokeratin-19-antibody-a53-ba2-cytoskeleton-marker-ab7754.html>.

Anti-Cytokeratin 19; abcam; ab52625; dilution 1:100; <https://www.abcam.com/cytokeratin-19-antibody-ep1580y-cytoskeleton-marker-ab52625.html>.

Anti-SOX2; abcam; ab15830; dilution 1:100; <https://www.abcam.com/sox2-antibody-ab15830.html>.

Anti-SOX2; R&D; AF2018; dilution 1:100; https://resources.rndsystems.com/pdfs/datasheets/af2018.pdf?v=20221029&_ga=2.31979961.663064109.1667061858-1717995244.1667061858.

Anti-NKX2.1; abcam; ab72876; dilution 1:100; <https://www.abcam.com/ttf1-antibody-8g7g31-ab72876.html>.

Anti-Cytokeratin 5; Thermo Fisher; MA5-17057; dilution 1:100; <https://www.thermofisher.com/antibody/product/Cytokeratin-5-Antibody-clone-2C2-Monoclonal/MA5-17057>.

Anti-Surfactant protein C; Merck Millipore; AB3786; dilution 1:300; https://www.merckmillipore.com/GB/en/product/Anti-Prosurfactant-Protein-C-proSP-C-Antibody,MM_NF-AB3786.

Anti-Acetylated alpha tubulin; Sigma; T7451; dilution 1:500; <https://www.sigmaaldrich.com/GB/en/product/sigma/t7451>.

Anti-CD31; Novus biological; NB100-2284; dilution 1:100; https://www.novusbio.com/products/cd31-pecam-1-antibody_nb100-2284.

Anti-CD31; abcam; ab119339; dilution 1:100; <https://www.abcam.com/cd31-antibody-hec7-ab119339.html>.

Anti-Alpha smooth muscle actin; abcam; ab124964; dilution 1:100; <https://www.abcam.com/alpha-smooth-muscle-actin-antibody-epr5368-ab124964.html>.

Anti-SARS-CoV spike glycoprotein; abcam; ab273433; dilution 1:100; <https://www.abcam.com/sars-spike-glycoprotein-antibody-1a9-ab273433.html>.

Anti-SARS-CoV-2 nucleocapsid; Sino Biological; 40143-R019; dilution 1:100; <https://www.sinobiological.com/antibodies/cov-nucleocapsid-40143-r019>.

Anti-SOX17; R&D; AF1924; dilution 1:100; https://resources.rndsystems.com/pdfs/datasheets/af1924.pdf?v=20221029&_ga=2.206978708.663064109.1667061858-1717995244.1667061858.

Anti-FXR; Novus biological; NBP2-16550; dilution 1:100; https://www.novusbio.com/products/foxr-nr1h4-antibody_nbp2-16550.

Anti-FXR; Santa Cruz; sc-25309 X; dilution 1:100; <https://datasheets.scbt.com/sc-25309.pdf>.

Anti-Actin; abcam; ab208080; dilution 1:100; <https://www.abcam.com/alexa-fluor-555-actin-antibody-epr16769-ab208080.html>.

Eukaryotic cell lines

Policy information about cell lines

Cell line source(s)

Vero E6 cells (ATCC™ CRL – 1586) were kindly donated by Gordon Dougan's laboratory. HEK293 cells (ATCC™ CRL – 1573) and HEK293T cells (ATCC™ CRL – 3216) were kindly donated by Nicholas J Mathenson's laboratory. Primary human tissues were used to derive organoids. All human tissues were obtained with full ethical approval (REC reference numbers: 12/EE/0253, NRES Committee East of England, Cambridge Central and 15/EE/0152 NRES Committee East of England, Cambridge South) and informed consent from the patients or the donors' families.

Authentication

None of the cell lines used were authenticated

Mycoplasma contamination

All line tested negative for mycoplasma.

Commonly misidentified lines (See [ICLAC](#) register)

No commonly misidentified cell lines were used in the study.

Animals and other organisms

Policy information about studies involving animals; ARRIVE guidelines recommended for reporting animal research

Laboratory animals

FVB/N female mice aged between 9 and 12 weeks were used. Golden Syrian Hamsters were purchased from Janvier Labs (France). Age matched male hamsters weighing between 80 – 100g were used. All animals were housed in a 12 hours/12 hours dark/light cycle, with a humidity of 45-65% and temperature of 20-24°C.

Wild animals

No wild animals were used in the study.

Field-collected samples

No field collected samples were used in the study.

Ethics oversight

The mouse study was approved by the Animal Ethics Committee of the Medical University of Vienna and the Federal Ministry of Science, Research and Economy (BMWFW-66.009/0008-WF/3b/2015) and was performed according to the Animal Research: Reporting of In Vivo Experiments (ARRIVE) guidelines.
The hamster study was performed in accordance with the UK Home Office Animals Scientific Procedures Act (ASPA, 1986). Additionally, all studies were approved by the University of Liverpool Animal Welfare and Ethical Review Board and performed under UK Home Office licences PP9284915 and PP4715265.

Note that full information on the approval of the study protocol must also be provided in the manuscript.

Human research participants

Policy information about [studies involving human research participants](#)

Population characteristics	Population characteristics of the human research participants are listed in Supplementary Table S5, Supplementary Table S6, Supplementary Table S7 and Supplementary Table S8.
Recruitment	Existing samples or datasets were used (e.g., data from COVID-Hep.net and SECURE-Liver registries, serum samples from the UK-PBC Cohort study, data from the VOCAL cohort). For the study involving volunteers from the University Medical Centre Hamburg-Eppendorf, following approval by local ethics committee (Ethik-Kommission der Ärztekammer Hamburg; Ref.No. 2021-300121-WF), the study was advertised in the University Medical Centre Hamburg-Eppendorf amongst clinicians regularly prescribing UDCA, and thus familiar with the drug and its possible side-effects. 8 clinicians who volunteered to participate in the study were recruited following informed consent. We appreciate the potential for selection and confounding bias in any study which is not a clinical trial, and this limitation is clearly stated in the results and discussion sections.
Ethics oversight	The COVID-Hep.net and SECURE-Liver registries data were deemed not to constitute human research by Clinical Trials and Research Governance at the University of Oxford (https://covid-hep.net/img/CTRG_COVID-Hep_20200402.pdf) and by the Institutional Review Board of University of North Carolina (https://covidcirrhosis.web.unc.edu/faq/) respectively. The study involving volunteers from the University Medical Centre Hamburg-Eppendorf was performed with informed consent and ethical approval from the Ethik-Kommission der Ärztekammer Hamburg (Ref.No. 2021-300121-WF). The study involving patients with PBC from the UK-PBC Nested Cohort was performed with informed consent and ethical approval from the National Research Ethics Committee (NREC) North West (14/NW/1146). The study involving patients from the VOCAL cohort was performed with informed consent and ethical approval from the Miami VA Institutional Review Board (Unique study approval ID 1477437-22).

Note that full information on the approval of the study protocol must also be provided in the manuscript.

Flow Cytometry

Plots

Confirm that:

- The axis labels state the marker and fluorochrome used (e.g. CD4-FITC).
- The axis scales are clearly visible. Include numbers along axes only for bottom left plot of group (a 'group' is an analysis of identical markers).
- All plots are contour plots with outliers or pseudocolor plots.
- A numerical value for number of cells or percentage (with statistics) is provided.

Methodology

Sample preparation	Cholangiocyte organoids obtained from intrahepatic ducts, common bile duct and gallbladder human tissues obtained from biopsies, deceased transplant organ donors or liver explants after obtaining informed consent were used. Organoids were harvested from Matrigel using Cell Recovery Solution for 20 minutes in ice. Organoids were treated with StemPro Accutase for 5 minutes at 37°C to dissociate cell clumps into single cells; fixed in 4% PFA for 20 minutes at 4°C; blocked with 10% donkey serum (Gibco) + 0.1% Triton-X in PBS (Gibco) for 30 minutes; stained with primary antibodies from abcam (See supplementary table S1) in 1% donkey serum (Gibco) + 0.1% Triton X in PBS (Gibco) for 1 hour at room temperature; primary antibody was subsequently washed in PBS (Gibco) for 5 minutes for three times; organoids were then stained with secondary antibodies (See supplementary table S1) for 1 hour at room temperature and filtered through a 40-µm filter and analysed. A detailed description of the protocol can be found in Methods section "Flow cytometry analyses".
Instrument	BD LSR-II from BD Biosciences.
Software	FlowJo version 10.
Cell population abundance	No post-sort fraction was collected. For each experiment at least 10.000 events were captured.
Gating strategy	Initial cell populations were gated using FSC and SSC to remove cell debris and large cell clumps. Subsequently, FSC-W and FSC-A were used to gate only single cells and remove doublets. This population was then used in fluorescent histograms. Samples stained for the secondary antibody only were used to set the gates. The gating strategy employed to analyse flow cytometry data can be found in Supplementary Figure S1.

- Tick this box to confirm that a figure exemplifying the gating strategy is provided in the Supplementary Information.